Elevated glycolytic metabolism of monocytes limits the generation of HIF-1α-driven migratory dendritic cells in tuberculosis

Mariano Maio[1,2,3], Joaquina Barros[1,2,3], Marine Joly[2,4], Zoi Vahlas[2,4], José Luis Marín Franco[1,2], Melanie Genoula[1,2], Sarah Monard[2,4], María Belén Vecchione[3], Federico Fuentes[1], Virginia Gonzalez Polo[3], María Florencia Quiroga[3], Mónica Vermeulen[1], Thien-Phong Vu Manh[5], Rafael J Argüello[5], Sandra Inwentarz[6], Rosa Musella[6], Lorena Ciallella[6], Pablo González Montaner[6], Domingo Palmero[6], Geanncarlo Lugo Villarino[2,4], María del Carmen Sasiain[1,2], Olivier Neyrolles[2,4], Christel Verollet[2,4,#], and Luciana Balboa[1,2,3,#,*]

[1] Instituto de Medicina Experimental (IMEX)-CONICET, Academia Nacional de Medicina, Buenos Aires, Argentina.

[2] International Associated Laboratory (LIA) CNRS IM-TB/HIV (1167), Buenos Aires, Argentina / International Research Project Toulouse, France

[3] Instituto de Investigaciones Biomédicas en Retrovirus y Sida (INBIRS), Consejo Nacional de Investigaciones Científicas y Técnicas (CONICET) - Universidad de Buenos Aires. Buenos Aires, Argentina

[4] Institut de Pharmacologie et de Biologie Structurale, Université de Toulouse, CNRS, UPS, Toulouse, France

[5] Aix Marseille University, CNRS, INSERM, CIML, Centre d'Immunologie de Marseille-Luminy, Marseille, France

[6] Instituto Prof. Dr. Raúl Vaccarezza and Hospital de Infecciosas Dr. F.J. Muñiz, Buenos Aires, Argentina

[#] These senior authors contributed equally to this work

* **Corresponding Author**: Luciana Balboa, Paraguay 2155, Piso 11 CABA (C1121ABG), Argentina. + 54(011) 4508-3689, luciana_balboa@hotmail.com

"The authors have declared that no conflict of interest exists."

Abstract

During tuberculosis, migration of dendritic cells (DCs) from the site of infection to the draining lymph nodes is known to be impaired, hindering the rapid development of protective T-cell mediated immunity. However, the mechanisms involved in the delayed migration of DCs during tuberculosis (TB) are still poorly defined. Here, we found that infection of DCs with *Mycobacterium tuberculosis* (Mtb) triggers HIF-1α-mediated aerobic glycolysis in a TLR2-dependent manner, and that this metabolic profile is essential for DC migration. In particular, the lactate dehydrogenase (LDH) inhibitor oxamate and the HIF-1α inhibitor PX-478 abrogated Mtb-induced DC migration *in vitro* to the lymphoid tissue-specific chemokine CCL21, and *in vivo* to lymph nodes in mice. Strikingly, we found that although monocytes from TB patients are inherently biased toward glycolysis metabolism, they differentiate into poorly glycolytic and poorly migratory DCs, compared with healthy subjects. Taken together, these data suggest that because of their preexisting glycolytic state, circulating monocytes from TB patients are refractory to differentiation into migratory DCs, which may explain the delayed migration of these cells during the disease and opens avenues for host-directed therapies for TB.

Graphical Abstract

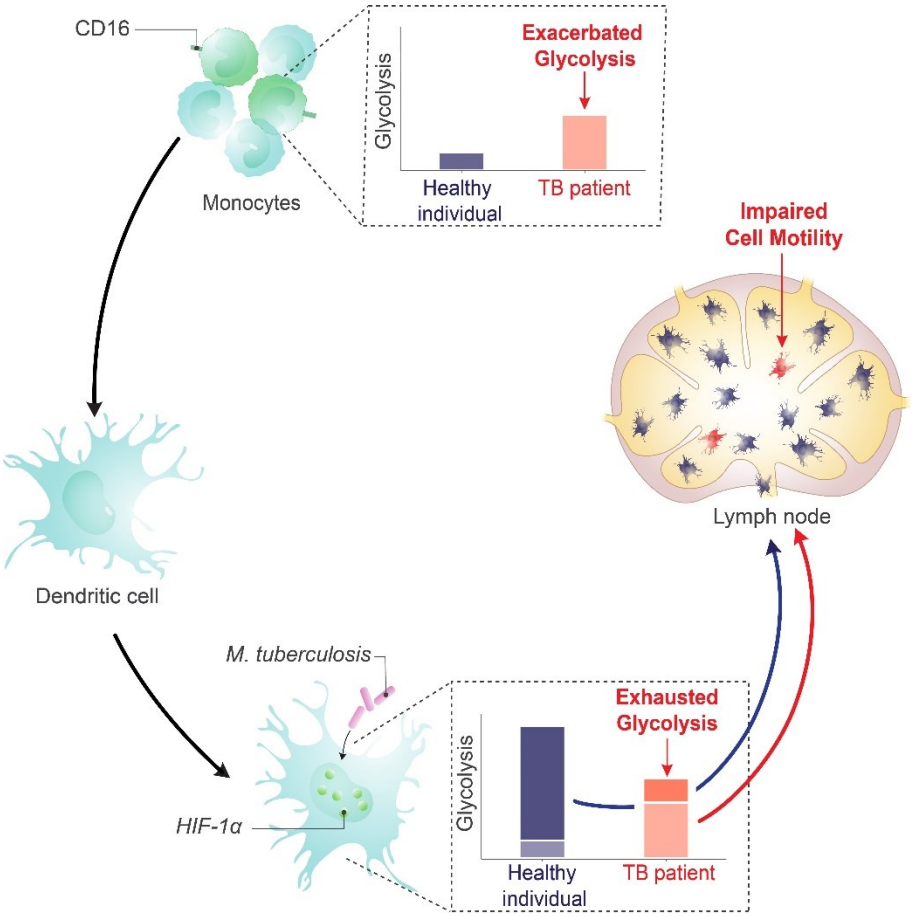

Introduction

Tuberculosis (TB) remains a major global health problem, responsible for approximately 1.6 million deaths annually. The causative agent of TB, *Mycobacterium tuberculosis* (Mtb), is a highly successful pathogen that has evolved several strategies to weaken the host immune response. Although reliable immune correlates of protective immunity against Mtb are still not well-defined, it is widely accepted that Th1 cells contribute to protection by secreting IFN-γ and promoting antimycobacterial activity in macrophages[1]. Importantly, the induction of a strong Th1 immune response relies on the generation of immunogenic dendritic cells (DCs) with strong migratory properties[2–5]. Mtb has been shown to interfere with several DC functions, thus impairing the induction and development of adaptive immunity[6–8]. For instance, we and others previously reported that Mtb-exposed DCs have low capacity for mycobacterial antigen presentation and stimulation of Mtb-specific $CD4^+$ T cells[9–13]. Additionally, Mtb-infected DCs were reported to have an impaired ability to migrate to lymph nodes *in vitro*[14,15] and *in vivo* in murine models[3,5]; however, the underlying molecular mechanisms of these phenotypes and their relevance to the migratory activity of monocyte-derived DCs in TB patients remain unknown.

Rapid, directed migration of DCs towards secondary lymphoid organs requires essential changes at the cellular and molecular levels[16]. Relatedly, the metabolic state of DCs is complex and varies according to cell origin, differentiation and maturation states, as well as local microenvironment, among other factors[17–20]. Studies have reported that upon pathogen sensing, the transcription factor hypoxia-inducible factor-1α (HIF-1α) increases glycolysis, which promotes immunogenic functions of DCs, such as IL-12 production, costimulatory marker expression[21], and cell migration[22–24]. By contrast, it was shown that HIF-1α represses the proinflammatory output of LPS-stimulated DCs and can inhibit DC-induced T-cell responses in other settings[25]. To reconcile these disparate roles for HIF-1α, it has been proposed that the impact of metabolic pathway activation on DC

86 functions varies among DC subsets[18]. To this point, most prior studies have been
87 conducted using murine conventional DCs and plasmacytoid DCs[19]. Recently, with the
88 implementation of high-dimensional techniques, it was demonstrated that distinct
89 metabolic wiring is associated with individual differentiation and maturation stages of
90 DCs[26], highlighting the importance of defining the metabolic profile of specific subsets of
91 DCs under physiological or pathological conditions[20]. Given the key role of DCs in the
92 host response to TB, it is thus crucial to investigate DC metabolism in the context of Mtb
93 infection[27].

94 We previously demonstrated that the TB-associated microenvironment, as conferred by
95 the acellular fraction of TB patient pleural effusions, inhibits HIF-1α activity leading to a
96 reduction in glycolytic and microbicidal phenotypes in macrophages[28]. Moreover,
97 activation of HIF-1α enhances Mtb control at early times post-infection in mouse
98 models[29], and this effect was associated with a metabolic switch of alveolar
99 macrophages towards an M1-like profile[28]. Given that HIF-1α activation promotes
100 protection at early stages of Mtb infection and given its role as a key regulator of DC
101 migration and inflammation[30], we hypothesized that HIF-1α could affect the functionality
102 of DCs in regulating the initiation and orchestration of the adaptive immune response to
103 Mtb, a process known to be delayed upon Mtb infection[5,6]. Here, we show that HIF-1α-
104 mediated glycolysis promotes DC activation and migration in the context of TB.
105 Importantly, we report active glycolysis in monocytes from TB patients, which leads to
106 poor glycolytic induction and migratory capacities of monocyte-derived DCs.

107 **Results**

108 **Mtb impacts metabolism in human monocyte-derived DCs**

109 To determine the impact of Mtb on the metabolism of human monocyte-derived DCs
110 (Mo-DCs), we assessed metabolic parameters associated with glycolysis and
111 mitochondrial changes upon Mtb stimulation or infection. Cells undergoing aerobic
112 glycolysis are characterized by increased consumption of glucose and the production
113 and release of lactate. We measured lactate release and glucose consumption in Mo-
114 DCs stimulated for 24 h with equivalent doses of either irradiated (iMtb) or viable Mtb.
115 DCs treated with either iMtb or viable Mtb released increased levels of lactate and
116 consumed more glucose than untreated DCs (**Figure 1A-B**). Consistently, both iMtb
117 treatment and Mtb infection resulted in an increase in expression of the key glycolysis-
118 activating regulator HIF-1α at both mRNA and protein levels (**Figure 1C-D**). Expression
119 of the gene encoding the glycolytic enzyme lactate dehydrogenase A (*LDHA*), which
120 catalyzes the conversion of lactate to pyruvate, was also increased in iMtb-treated or
121 Mtb-infected DCs (**Figure 1E**). In agreement with their enhanced glycolysis profile, DCs
122 stimulated with iMtb or infected with viable Mtb had increased expression of the glucose
123 transporter GLUT1 (SLC2A1)[31] (**Figure 1F)**. Of note, *LDHA* and *GLUT1* are HIF-1α
124 target genes, and their upregulation correlated with the increase in HIF-1α expression
125 upon Mtb stimulation. To assess changes in the mitochondria, we measured
126 mitochondrial mass and morphology. We found a higher mitochondrial mass as well as
127 larger individual mitochondria in iMtb-stimulated DCs compared to untreated DCs
128 (**Figure 1G-H**). In contrast to the findings obtained upon iMtb stimulation, Mtb-infected
129 DCs displayed a reduction in their mitochondrial mass (**Figure 1G**). This result indicates
130 that although both Mtb-infected and irradiated Mtb-exposed DCs show a clear increase
131 in their glycolytic activity, divergent responses are observed in terms of mitochondrial
132 mass. Therefore, our data indicate that Mtb impacts the metabolism of Mo-DCs, leading
133 to mitochondrial changes and triggering glycolysis-associated parameters.

134

135 **Mtb exposure shifts DCs to a glycolytic profile over oxidative phosphorylation**

136 To further characterize the metabolic profile of DCs upon iMtb-stimulation or Mtb-
137 infection, we next evaluated the metabolism of DCs at single-cell level using the
138 SCENITH technology[32]. This method is based on a decrease in ATP levels that is tightly
139 coupled with a decrease in protein synthesis and displays similar kinetics[32]. By treating
140 the cells with glucose or mitochondrial respiration inhibitors, and measuring their impact
141 on protein synthesis by puromycin incorporation via flow cytometry, glucose and
142 mitochondrial dependences can be quantified. Two additional derived parameters such
143 as “glycolytic capacity” and “fatty acid and amino acid oxidation (FAO & AAO) capacity”
144 were also calculated. SCENITH technology revealed a lower reliance on oxidative
145 phosphorylation (OXPHOS) in parallel with an increase in the glycolytic capacity of iMtb-
146 stimulated (**Figure 2A-B),** Mtb-infected DCs and even bystander DCs (those cells that
147 are not directly infected but stand nearby) (**Figure 2C-D**). Since bystander DCs are not
148 in direct association with Mtb (Mtb-RFP- DCs), soluble mediators induced in response
149 to infection may be sufficient to trigger glycolysis even in uninfected cells. No differences
150 were observed for glucose dependence and FAO & AAO capacity (**Figure 2A-D**).
151 Additionally, we found no changes between the FAO dependency in Mtb-stimulated DCs
152 in comparison to control cells when the FAO inhibitor (etomoxir) was used (**Figure S1A**).
153 For the case of iMtb-stimulated DCs, we also assessed the intracellular rates of glycolytic
154 and mitochondrial ATP production using Seahorse technology. Bioenergetic profiles
155 revealed that iMtb increased the rate of protons extruded over time, or proton efflux rate
156 (PER), as well as the basal oxygen consumption rate (OCR) in Mo-DCs (**Figure 2E**).
157 The measurements of basal extracellular acidification rate (ECAR) and OCR were used
158 to calculate ATP production rate from glycolysis (GlycoATP) and mitochondrial OXPHOS
159 (MitoATP). The ATP production rates from both glycolysis and mitochondrial respiration
160 were augmented upon iMtb-stimulation (**Figure 2F**). Similar to SCENITH results, the
161 relative contribution of GlycoATP to overall ATP production was increased, while

162 MitoATP contribution was decreased in iMtb-treated cells compared to untreated cells
163 (**Figure 2G**). These results confirmed the change in DC metabolism induced by Mtb,
164 with an increase in the relative glycolytic contribution to overall metabolism at the
165 expense of the OXPHOS pathway. Together, metabolic profiling indicates that a
166 metabolic switch toward aerobic glycolysis occurs in Mo-DCs exposed to Mtb.
167

168 **Mtb triggers the glycolytic pathway through TLR2 ligation**

169 Since Mtb is sensed by Toll-like receptors (TLR)-2 and -4[33], we investigated the
170 contribution of these receptors to glycolysis activation in Mo-DCs upon Mtb stimulation.
171 Using specific neutralizing antibodies for these receptors, we found that TLR2 ligation,
172 but not that of TLR4, was required to trigger the glycolytic pathway, as reflected by a
173 decrease in lactate release, glucose consumption and HIF-1α expression in iMtb-
174 stimulated DCs treated with an anti-TLR2 antibody (**Figure 3A-C**). As a control, and as
175 expected given the reliance on TLR4 for LPS sensing[34], lactate release and glucose
176 consumption were abolished in LPS-stimulated DCs in the presence of neutralizing
177 antibodies against TLR4 but not TLR2 (**Figure S2A-B**). Moreover, blockade of TLR2
178 also diminished glycolytic ATP production in iMtb-stimulated DCs without altering
179 OXPHOS-associated ATP production (**Figure 3D**) or the size and morphology of
180 mitochondria (**Figure S2C**), suggesting that TLR2 engagement by iMtb is required for
181 the induction of glycolysis but not mitochondrial respiration. Interestingly, TLR2 ligation
182 was also necessary for lactate release and HIF-1α up-regulation triggered by viable Mtb,
183 (**Figure S2D-E**). To further confirm the involvement of TLR2 in the induction of glycolysis,
184 we tested the effect of synthetic (Pam_3CSK_4) or mycobacterial (peptidoglycans, PTG)
185 TLR2 agonists[35,36] and found that both ligands induced lactate release and glucose
186 consumption in DCs (**Figure 3E-F**), without affecting cell viability (**Figure S2F**). Thus,
187 our data indicate that Mtb induces glycolysis in Mo-DCs through TLR2 engagement.
188

189 **HIF-1α is required for DC maturation upon iMtb stimulation but not for CD4⁺ T**
190 **lymphocyte polarization**

191 To determine the impact of glycolysis on DC maturation and the capacity to activate T
192 cells, we inhibited HIF-1α activity in iMtb-stimulated DCs employing two HIF-1α inhibitors
193 that display different mechanisms of action. The first is PX-478 (PX) that lowers HIF-1α
194 levels by inhibiting HIF-1α deubiquitination, decreases HIF-1α mRNA expression, and
195 reduces HIF-1α translation[37]; the second one is echinomycin (Ech), which inhibits the
196 binding of HIF-1α to the hypoxia response element thereby blocking HIF-1α DNA binding
197 capability[38,39]. Treatment with either HIF-1α inhibitor PX or Ech diminished lactate release
198 and glucose consumption in iMtb-stimulated DCs without affecting cell viability at the
199 indicated concentration (**Figure S3A-F**). HIF-1α inhibition by PX significantly abolished
200 ATP production associated with glycolysis without affecting absolute levels of OXPHOS-
201 derived ATP production in iMtb-stimulated DCs (**Figure 4A and Figure S3G**). In line with
202 these results, the glycolytic capacity was reduced in iMtb-stimulated DCs treated with
203 Ech (**Figure S3H**). Although HIF-1α inhibitors did not affect the uptake of iMtb by DCs
204 (**Figure S3I**), we observed a reduction in the expression of activation markers CD83 and
205 CD86, but not in the inhibitory molecule PD-L1, upon treatment with PX (**Figure 4B**) or
206 Ech (**Figure S4**)**.** We then measured cytokine production in iMtb-stimulated DCs after
207 HIF-1α inhibition and noted a reduction in TNF-α and an increase in IL-10 production by
208 PX-treated cells (**Figure 4C**). To assess the capacity of DCs to activate T cells in
209 response to mycobacterial antigens, we co-cultured DCs and autologous CD4⁺ T cells
210 from PPD⁺ donors in the presence or absence of HIF-1α inhibitors and measured the
211 overall IFN-γ and IL-17 production in culture supernatants as well as cell surface
212 expression of T cell markers. We found no significant differences in the activation profile
213 of autologous CD4⁺ T cells in coculture with iMtb-stimulated DCs treated or not with PX
214 (**Figure 4D-E and Figure S5**). We conclude that while HIF-1α is important for the
215 maturation of iMtb-stimulated Mo-DCs, it does not influence their capacity to activate
216 CD4⁺ T cells, at least *in vitro*.

217

218 **HIF-1α-mediated glycolysis triggers the motility of DCs upon iMtb stimulation**

219 Since DC migration to lymph nodes is essential to initiate an adaptive immune response
220 and glycolytic activity has been reported to control DC migration upon stimulation[22,23], we
221 evaluated the migratory properties of iMtb-stimulated DCs in the presence of inhibitors
222 of HIF-1α and LDH which catalyzes the interconversion of pyruvate and lactate. First, we
223 confirmed that PX and oxamate (OX), a well-established LDH inhibitor, diminished the
224 glycolytic activity of iMtb-stimulated human Mo-DCs, as demonstrated by reduced lactate
225 release (**Figure S3A and 5A**). Next, using a transwell migration assay, we found that
226 PX and OX treatment significantly diminished the chemotactic activity of iMtb-stimulated
227 human Mo-DCs in response to CCL21 (**Figure 5B**), a CCR7 ligand responsible for the
228 migration of DCs into lymphoid organs. We also assessed the 3 dimensional (3D)
229 migration capacity of iMtb-stimulated DCs through a collagen matrix in which DCs use
230 an amoeboid migration mode[40] and found that 3D migration was significantly impaired
231 upon HIF-1α or glycolysis inhibition (**Figure 5C**). The role of glycolysis in the migration
232 of iMtb-stimulated Mo-DCs was further confirmed using an additional LDHA inhibitor,
233 GSK2837808A, which reduced both the release of lactate by iMtb-stimulated Mo-DCs
234 and their migration in response to CCL21 (**Figure S6A-B**). Attenuation of cell migration
235 through collagen induced by OX and PX was also confirmed in Mtb-infected DCs (**Figure**
236 **5D**). To further investigate the effects of glycolysis on cell migration, we turned to an *in*
237 *vivo* model. Murine bone marrow-derived DCs (BMDCs) isolated and stimulated with
238 iMtb in the presence or absence of PX or OX were labeled with CFSE and transferred
239 into naïve mice (**Figure 5E**). Similar to human Mo-DCs, iMtb stimulation increased
240 glycolysis in BMDCs, which was inhibited by PX and OX treatment *in vitro* (**Figure S6C**).
241 Three hours after the transfer of BMDCs into recipient mice, nearby lymph nodes were
242 collected for DC quantification (**Figure 5E**). A higher number of adoptively transferred
243 DCs (CFSE-labeled $CD11c^+$ cells) were detected in lymph nodes from mice that received
244 iMtb-stimulated BMDCs compared to mice that received untreated BMDCs or iMtb-

245 BMDCs treated with either PX or OX (**Figure 5F and Figure S6D**). Of note, we verified
246 that CCR7 expression on iMtb-stimulated BMDCs was not affected by OX or PX
247 treatment, so the effect could not be ascribed to downregulation of the chemokine
248 receptor (**Figure S6E**). Therefore, we conclude that HIF-1α-mediated glycolysis is
249 required for the successful migration of iMtb-stimulated DCs into lymph nodes.
250

251 **Stabilization of HIF-1α promotes migration of tolerogenic DCs and DCs derived**
252 **from TB patient monocytes**

253 Since DC differentiation is skewed, at least partially, towards a tolerogenic phenotype
254 during TB[41–43], we investigated whether tolerogenic DCs can be reprogrammed into
255 immunogenic DCs by modulating their glycolytic pathway after iMtb stimulation. To this
256 end, we generated tolerogenic Mo-DCs by adding dexamethasone (Dx) before
257 stimulation with iMtb in the presence or absence of dimethyloxalylglycine (DMOG), which
258 stabilizes the expression of HIF-1α. HIF-1α expression is tightly regulated by prolyl
259 hydroxylase domain containing proteins which facilitate the recruitment of the von
260 Hippel-Lindau (VHL) protein, leading to ubiquitination and degradation of HIF-1α by the
261 proteasomes[44]. DMOG inhibits the prolyl hydroxylase domain-containing proteins.
262 Acquisition of the tolerogenic phenotype was confirmed by the lack of upregulation of
263 costimulatory markers CD83 and CD86, as well as by increased PD-L1 expression in
264 iMtb-DCs treated with Dx compared to control iMtb-DCs (**Figure S7A**). Moreover, Dx-
265 treated DCs did not exhibit an increase in lactate release, consumption of glucose or
266 induction of HIF-1α expression in response to iMtb, showing a high consumption of levels
267 of glucose under basal conditions (**Figure 6A-B**). Of note, HIF-1α stabilization using
268 DMOG restored the HIF-1α expression and lactate production in response to iMtb in Dx-
269 treated DCs and increased the consumption of glucose (**Figure 6A-B**). Activation of HIF-
270 1α also improved 3D amoeboid migration, as well as 2D migration capacity of DCs
271 towards CCL21 of iMtb-stimulated Dx-treated DCs (**Figure 6C-D and Figure S7B**).
272 Confirming the relevance of these findings to human TB patients, we found that iMtb-

273 stimulated Mo-DCs from TB patients were deficient in their capacity to migrate towards
274 CCL21 (**Figure 6E**) and in glycolytic activity, compared to Mo-DCs from healthy subjects
275 (**Figure 6F-G**). Strikingly, stabilizing HIF-1α expression using DMOG in Mo-DCs from
276 TB patients restored their chemotactic activity in response to iMtb (**Figure 6H**). These
277 data indicate that the impaired migratory capacity of iMtb-stimulated tolerogenic DCs or
278 TB patient-derived DCs can be restored via HIF-1α stabilization; thus, glycolysis is critical
279 for DC function during TB in both murine and human contexts.
280

281 **CD16^{+} monocytes from TB patients show increased glycolytic capacity**

282 Since we observed differences in the metabolic activity of DCs derived from monocytes
283 of TB patients when compared to healthy donors, we next focused on evaluating the
284 release of lactate by DC precursors from both subject groups during the first hours of DC
285 differentiation with IL-4/GM-CSF. We found a high release of lactate by monocytes from
286 TB patients compared to healthy donors after 1 h of differentiation (**Figure 7A**). Lactate
287 accumulation increased in both subject groups after 24 h with IL-4/GM-CSF (**Figure 7A**).
288 Based on these differential glycolytic activities displayed by DC precursors from both
289 subject groups at very early stages of the differentiation process, we decided to evaluate
290 the *ex vivo* metabolic profile of monocytes using SCENITH. To this end, we assessed
291 the baseline glycolytic capacity of the three main populations of monocytes: classical
292 (CD14^{+}CD16^{-}), intermediate (CD14^{+}CD16^{+}), and non-classical (CD14^{dim}CD16^{+})
293 monocytes. We found that both populations of CD16^{+} monocytes from TB patients had
294 a higher glycolytic capacity than monocytes from healthy donors (**Figure 7B**). Moreover,
295 the glycolytic capacity of CD16^{+} monocytes (CD14^{+}CD16^{+} and CD14^{dim}CD16^{+})
296 correlates with time since the onset of TB-related symptoms (**Figure 7C**), with no
297 association to the extent or severity of lung disease (unilateral/bilateral lesions and
298 with/without cavities, **Figure S8**). To further expand the metabolic characterisation of
299 monocyte subsets from TB patients, we used previously published transcriptomic data
300 (GEO accession number: GSE185372) of CD14^{+}CD16^{-}, CD14^{+}CD16^{+} and

301 $CD14^{dim}CD16^{+}$ monocytes isolated from individuals with active TB, latent TB ($IGRA^{+}$), as
302 well as from TB negative healthy controls ($IGRA^{-}$)[45]. Within this framework, we performed
303 high-throughput GeneSet Enrichment Analysis (GSEA) using the BubbleMap module of
304 BubbleGUM, which includes a multiple testing correction step to allow comparisons
305 between the three monocyte subsets[46]. As expected, this approach reveals enrichments
306 in genes associated with interferon responses (alpha and gamma) in patients with active
307 TB compared to healthy donors (either $IGRA^{-}$ or latent TB) for all three monocyte subsets
308 (**Figure 7D**). Consistent with our findings, glycolysis increases in active TB in both
309 $CD14^{+}CD16^{+}$ and $CD14^{dim}CD16^{+}$ monocytes (albeit not significant), while it appears to
310 decrease in classical $CD14^{+}CD16^{-}$ monocytes (**Figure 7D**). Unlike $CD14^{+}CD16^{-}$ cells,
311 the inflammatory response is notably enriched in $CD14^{+}CD16^{+}$ and $CD14^{dim}CD16^{+}$
312 monocytes from patients with active TB compared those with latent TB or healthy
313 subjects (**Figure 7D**), suggesting that their glycolytic profile correlates with a higher
314 inflammatory state. Finally, no significant enrichment of oxidative phosphorylation-
315 associated genes was found in any of the performed comparisons (**Figure 7D**). Taken
316 together, these results demonstrate that TB disease is associated with an increased
317 activation and glycolytic profile of circulating $CD16^{+}$ monocytes.
318

319 **HIF1-α activation in $CD16^{+}$ monocytes from TB patients leads to differentiated DCs**
320 **with a poor migration capacity**

321 Since circulating $CD16^{+}$ monocytes from TB patients are highly glycolytic, we evaluated
322 the expression of HIF1-α among the populations. We found that $CD16^{+}$ monocytes from
323 TB patients exhibited a higher expression of HIF1-α than from healthy donors (**Figure**
324 **8A**). As we have previously demonstrated that $CD16^{+}$ monocytes from TB patients
325 generate aberrant DCs[41], we hypothesized that the different metabolic profile of this
326 monocyte subset could yield DCs with some sort of exhausted glycolytic capacity and
327 thus lower migration activity upon Mtb exposure. To test this hypothesis, we treated with

328 DMOG to increase the activity of HIF-1α during the first 24 h of monocyte differentiation
329 from healthy donors, leading to an exacerbated increase in lactate release at early
330 stages of the differentiation (**Figure 8B**). Such early addition of DMOG to healthy
331 monocytes resulted in the generation of DCs (6 days with IL-4/GM-CSF) characterized
332 by equivalent levels of CD1a as control DCs, with a significant decrease in the
333 expression of DC-SIGN (**Figure S9A**). In terms of activation marker expression, DCs
334 differentiated from DMOG-pretreated cells responded to iMtb by upregulating CD86 at
335 higher levels compared to control cells, with an accompanying trend towards reduced
336 upregulation of CD83 (**Figure S9B**). We also observed that DCs from DMOG pretreated-
337 cells exhibited a lower migratory capacity in response to iMtb (**Figure 8C**), reminiscent
338 of the 2D migration capacities of Mo-DCs from TB patients. Altogether, our data suggest
339 that the activated glycolytic status of monocytes from TB patients leads to the generation
340 of DCs with low motility in response to Mtb.
341
342

343 **Discussion**

344 In this study, we provide evidence for the role of HIF-1α-mediated glycolysis in promoting
345 the migratory capacity of DCs upon encounter with iMtb. Our approach to quantify the
346 *ex vivo* metabolism of monocytes shows that CD16$^+$ monocytes from TB patients display
347 an exacerbated glycolytic activity that may result in the generation of DCs with poor
348 migratory capacities in response to iMtb. Our results suggest that under extensive
349 chronic inflammatory conditions, such as those found in TB patients, circulating
350 monocytes may be metabolically preconditioned to differentiate into DCs with low
351 migratory potential.

352

353 Upon Mtb infection of naive mice, initial accumulation of activated CD4$^+$ T cells in the
354 lung is delayed, occurring between 2-3 weeks post-infection[3,47]. The absence of
355 sterilizing immunity induced by TB vaccines, such as BCG, has been proposed to result
356 from delayed activation of DCs and the resulting delay in antigen presentation and
357 activation of vaccine-induced CD4$^+$ T-cell responses[48]. In this context, it was
358 demonstrated that Mtb-infected Mo-DCs recruited to the site of infection exhibit low
359 CCR7 expression and impaired migration to lymph nodes compared to uninfected Mo-
360 DCs[49]. Additionally, Mo-DCs have been found to play a key role in transporting Mtb
361 antigens from the lung to the draining lymph node, where conventional DCs present
362 antigens to naive T cells[50]. The migratory capacity of responding DCs is thus of
363 paramount importance to the host response to Mtb infection.

364

365 Here, we found that Mtb exposure triggers glycolysis in Mo-DCs from healthy donors,
366 which promotes their migration capacity in a HIF-1α-dependent manner. Recently, it was
367 shown that glycolysis was required for CCR7-triggered murine DC migration in response
368 to LPS[22–24]. Glycolysis was also reported to be required for the migration of other immune
369 cells such as macrophages[51] and regulatory T cells[52]. Consistently, we show that

370 inhibition of HIF-1α-dependent glycolysis impairs human Mo-DC migration upon Mtb
371 stimulation. The link between cellular metabolism and migratory behavior are supported
372 by studies that have elucidated how glycolysis can be mechanically regulated by
373 changes in the architecture of the cytoskeleton, ultimately impacting the activity of
374 glycolytic enzymes[53,54]. In addition, interesting links between cellular mechanics and
375 metabolism have been previously described for DCs, highlighting the potential to alter
376 DC mechanics to control DC trafficking and consequently T cell priming[16]. However,
377 studies focused on the molecular mechanisms by which metabolic pathways impact the
378 machinery responsible for cell movement in the context of TB infection will be required
379 to better understand and design therapeutic manipulation.
380
381 Our research indicates that DCs exhibit upregulated glycolysis following stimulation or
382 infection by Mtb. This metabolic shift is crucial for facilitating cell migration to the draining
383 lymph nodes, an essential step in mounting an effective immune response. Yet, it
384 remains uncertain whether this glycolytic induction reaches a threshold conducive to
385 generating a protective immune response, a matter that our findings do not definitively
386 address. In addition, we demonstrated that tolerogenic DCs induced by dexamethasone
387 as well as DCs derived from TB patient monocytes exhibit lower lactate release and
388 impaired trafficking toward CCL21 upon Mtb stimulation; both phenotypes could be
389 rescued by stabilization of HIF-1α expression. To our knowledge, this is the first study to
390 address how the metabolic status of monocytes from TB patients influences the
391 migratory activity of further differentiated DCs. According to our findings, the activation
392 status of the glycolysis/HIF-1α axis in monocytes would be a predictor of refractoriness
393 to differentiation into migratory DCs in TB. With respect to the metabolism of tolerogenic
394 DCs broadly, our results are consistent with reported data showing that DC tolerance
395 can be induced by drugs promoting OXPHOS, such as vitamin D and dexamethasone[55–
396 57]. It was interesting to note that, although migration of tolerogenic DCs did not increase

397 upon Mtb stimulation, it was increased under basal conditions, which agrees with
398 previous data showing a high steady-state migration capacity of putatively tolerogenic
399 DCs[58].
400
401 It has been widely demonstrated that immune cells can switch to glycolysis following
402 engagement of TLRs[59]. Our work showed that TLR2 ligation by either viable or irradiated
403 Mtb was necessary to trigger glycolysis in DCs, at least at early times post-stimulation.
404 In fact, even bystander DCs increased their glycolytic activity in Mtb-infected cultures,
405 suggesting that mycobacterial antigens or bacterial debris present in the
406 microenvironment may be sufficient to trigger TLR-dependent glycolysis. In the context
407 of natural infection *in vivo*, we foresee that DC with different levels of infection will coexist,
408 some with low bacillary load that, according to our data, may be able to trigger glycolysis
409 and migrate, while others highly infected DCs would more likely die[60]. It remains to be
410 elucidated whether persistent interaction between DCs and Mtb might lead to an
411 attenuation in glycolysis over time, as has been reported for macrophages[61]. In this
412 regard, our data demonstrates that chronic Mtb infection leads to monocytes bearing an
413 exacerbated glycolytic status likely tied to prolonged and or excessive stimulation of
414 membrane bound TLRs in circulation, which results in DCs with an exhausted glycolytic
415 capacity. Although DCs stimulated with iMtb in the presence of a HIF-1α inhibitor
416 exhibited differences in activation markers and cytokine profile, we found that they were
417 still able to activate $CD4^+$ T cells from PPD+ donors in response to iMtb. These findings
418 complement previous evidence showing that LPS-induced mature DCs inhibit T-cell
419 responses through HIF-1α activation in the presence of glucose, leading to greater T cell
420 activation capacity in low glucose contexts such as at the interface between DCs and T
421 cells[25]. In this work, we did not detect an impact on T cell activation upon HIF-1α inhibition
422 in DCs, but we observed a clear reduction in their migration capacity that may limit or
423 delay DC encounters with T cells *in vivo*, leading to poor T cell activation in the lymph

424 nodes. In this regard, mouse studies have shown that DC migration directly correlates
425 with T cell proliferation[62]. However, we cannot rule out the possibility that other $CD4^+$ T
426 cell subsets (such as regulatory T cells), CD1-restricted T cells, and/or $CD8^+$ T cell
427 subsets could be differentially activated by iMtb-stimulated DCs lacking HIF-1α activity.
428
429 Three different populations of human monocytes have been identified: classical ($CD14^+$,
430 $CD16^-$), intermediate ($CD14^+$, $CD16^+$), and non-classical ($CD14^{dim}$, $CD16^+$) monocytes[63].
431 These monocyte subsets are phenotypically and functionally distinct. Classical
432 monocytes readily extravasate into tissues in response to inflammation, where they can
433 differentiate into macrophage-like or DC-like cells[64]; intermediate monocytes are well-
434 suited for antigen presentation, cytokine secretion, and differentiation; and non-classical
435 monocytes are involved in complement and Fc gamma-mediated phagocytosis and their
436 main function is cell adhesion[65,66]. Unlike non-classical monocytes, the two $CD14^+$
437 monocyte populations are known to extravasate into tissues and thus are likely to act as
438 precursors capable of giving rise to Mo-DCs in inflamed tissues. However, the DC
439 differentiation capacity of the intermediate population is still not well defined. We
440 previously demonstrated that monocytes from TB patients generate aberrant DCs, and
441 that $CD16^+$ monocytes generate aberrant DCs upon treatment with GM-CSF and IL-4[41].
442 Here, we demonstrated that glycolysis seems to play a dual role during DC differentiation
443 from monocytes, on the one side, being required for fully differentiated-DC migration to
444 lymph nodes in response to Mtb and, on the other side, leading to DCs with poor iMtb-
445 responsive migratory capacity if activated during the onset of DC differentiation. In this
446 regard, DCs from healthy subjects respond to iMtb by inducing a glycolytic and migratory
447 profile, while monocytes isolated from TB patients exhibit an unusual early glycolytic
448 state that results in the ulterior generation of DCs with low glycolytic and migratory
449 activities in response to Mtb. Similarly, we found that $CD16^+$ cells from TB patients
450 display an activated glycolytic status, as well as elevated HIF-1α expression levels

451 compared to their healthy counterparts. Additionally, we showed that monocytes from
452 TB patients are not only enriched in CD16^{+} cells, but also display an altered chemokine
453 receptor expression profile[67], demonstrating that both phenotype and function of a given
454 monocyte subset may differ under pathological conditions. While it is difficult to
455 determine whether the heightened glycolytic profile of monocytes may limit their
456 differentiation into DCs *in vivo*, we provided evidence that an increase in HIF1α-mediated
457 glycolysis in precursors leads to the generation of cells with poor ability to migrate in
458 response to CCL21 *in vitro.* In line with this observation, a recent study revealed a
459 significant increase in the glycolytic capacity occurs during the first 24 h of monocyte
460 differentiation towards a tolerogenic DC phenotype, as induced by vitamin D3[26],
461 highlighting the detrimental role of an early activated inflammatory profile in DC
462 precursors. A possible explanation for these effects may be found in lactate
463 accumulation in monocytes during DC differentiation. Lactate signaling in immune cells
464 leads to metabolic alterations in DCs that program them to a regulatory state[68], and
465 lactate has also been shown to suppress DC differentiation and maturation[18]; thus,
466 excessive precursor glycolytic activity may result in DCs biased toward regulatory
467 functions.
468
469 Taken together, our data offer new insights into the immunometabolic pathways involved
470 in the trafficking of DCs to the lymph nodes. These insights may have various
471 implications depending on factors such as timing, cell type, and location induction of the
472 HIF1α/glycolysis axis. On the one hand, nurturing HIF-1α-mediated glycolytic activity in
473 DCs during the early stages of infection could potentially enhance the effectiveness of
474 preventive strategies for TB. Particularly noteworthy is the significant impact revealed in
475 studies where the number of DCs reaching the lymph node proved to be a crucial factor
476 in determining the success of DC-based vaccination[62]. On the other hand, premature
477 activation of glycolysis in precursors, as observed in CD16+ monocytes from severe TB

patients, could disrupt the delicate balance necessary for an optimal immune response. This variability is consistent with the paradigm of "too much, too little," as demonstrated by the dual roles of IFNγ[69] and TNFα[70] in the context of TB. It also underscores the vital importance of maintaining an equilibrium in inflammatory responses. This study lays the foundation for further exploration into the potential systemic impact of the HIF1α/glycolysis axis within the realm of chronic inflammation contrasting with its role in a local setting during the acute phase of infection. By enhancing our understanding, these findings aim to guide the development of innovative preventive and therapeutic strategies for TB.

487 **Methods**

488 **Chemical Reagents**

489 LPS from Escherichia coli O111:B4 was obtained from Sigma-Aldrich (St. Louis, MO,
490 USA). Dexamethasone (Dx) was from Sidus (Buenos Aires, Argentina). PX-478 2HCL
491 was purchased from Selleck Chemicals (Houston, USA) and DMOG from Santa Cruz,
492 Biotechnology (Palo Alto, CA, USA). Additionally, GSK2837808A was purchased from
493 Cayman Chemical (Michigan, USA) together with echinomycin and sodium oxamate.

494

495 **Bacterial strain and antigens**

496 Mtb H37Rv strain was grown at 37°C in Middlebrook 7H9 medium supplemented with
497 10 % albumin-dextrose-catalase (both from Becton Dickinson, New Jersey, USA) and
498 0.05 % Tween-80 (Sigma-Aldrich). The Mtb γ-irradiated H37Rv strain (NR-49098) was
499 obtained from BEI Resource (NIAID, NIH, USA). The RFP-expressing Mtb strain was
500 gently provided by Dr. Fabiana Bigi (INTA, Castelar, Argentina).

501

502 **Preparation of monocyte-derived DCs**

503 Buffy coats from healthy donors were prepared at Centro Regional de Hemoterapia
504 Garrahan (Buenos Aires, Argentina) according to institutional guidelines (resolution
505 number CEIANM-664/07). Informed consent was obtained from each donor before blood
506 collection. Monocytes were purified by centrifugation on a discontinuous Percoll gradient
507 (Amersham, Little Chalfont, UK) as previously described[71]. Then, monocytes were
508 allowed to adhere to 24-well plates at $5x10^5$ cells/well for 1 h at 37°C in warm RPMI-
509 1640 medium (ThermoFisher Scientific, Waltham, MA). The mean purity of adherent
510 monocytes was 85 % (range: 80-92 %). The medium was then supplemented to a final
511 concentration of 10 % Fetal Bovine Serum (FBS, Sigma-Aldrich), human recombinant
512 Granulocyte-Macrophage Colony-Stimulating Factor (10 ng/ml, GM-CSF, Peprotech,
513 New Jersey, USA) and IL-4 (20 ng/ml, Biolegend, San Diego, USA). Cells were allowed
514 to differentiate for 5-7 days (DC-SIGN$^+$ cells in the culture > 90 %).

515

516 **DC stimulation**

517 DCs were stimulated with either irradiated Mtb (iMtb) or viable Mtb at equivalent OD_{600}
518 doses for 24 h at 37 ºC. The cells were washed three times, and their phenotype and
519 functionality were evaluated together with survival of activated cells; cell number and
520 viability were determined by either trypan blue exclusion assays or MTT. Infections were
521 performed in the biosafety level 3 (BSL-3) laboratory at the Unidad Operativa Centro de
522 Contención Biológica (UOCCB), ANLIS-MALBRAN (Buenos Aires), according to the
523 biosafety institutional guidelines.

524

525 **DC treatments**

526 When indicated, neutralizing monoclonal antibodies (mAb), or their corresponding
527 isotype antibodies as mock controls, were added 30 min prior to DC stimulation to inhibit
528 TLR2 (309717, Biolegend) or TLR4 (312813, Biolegend). In addition, DCs were
529 incubated with PX-478 (20 μM) or Echinomycin (1 nM) with the purpose of inhibiting HIF-
530 1α activity, DMOG (50 μM) to stabilize HIF-1α, and oxamate (20 mM) or GSK2837808A
531 (20 μM) to inhibit LDH. DC stimulation with iMtb occurred 30 min after treatment without
532 drug washout.

533 In figure 6 and S6, dexamethasone-induced tolerogenic dendritic cells (Dx-DC) were
534 generated by incubating DCs with 0.1 μM of dexamethasone for 1 h. Thereafter, cells
535 were washed, and "complete medium" was added. Tolerogenic Dx-DCs were then
536 stimulated (or not) with iMtb in the presence or not of DMOG (50 μM).

537

538 **Determination of metabolite concentrations**

539 Lactate production and glucose concentrations in the culture medium was measured
540 using the spectrophotometric assays Lactate Kit and Glicemia Enzimática AA Kit both
541 from Wiener (Argentina), which are based on the oxidation of lactate or glucose,
542 respectively, and the subsequent production of hydrogen peroxide[72]. The consumption

543 of glucose was determined by assessing the reduction in glucose levels in culture
544 supernatants in comparison with RPMI 10 % FBS. The absorbance was read using a
545 Biochrom Asys UVM 340 Microplate Reader microplate reader and software.
546

547 **Quantitative RT-PCR**

548 Total RNA was extracted with Trizol reagent (Thermo Fisher Scientific) and cDNA was
549 reverse transcribed using the Moloney murine leukemia virus reverse transcriptase and
550 random hexamer oligonucleotides for priming (Life Technologies, CA, USA). The
551 expression of the genes *HIF-1α* and *LDH-A* was determined using the PCR SYBR Green
552 sequence detection system (Eurogentec, Seraing, Belgium) and the CFX Connect Real-
553 Time PCR Detection System (Bio-Rad, CA, USA). Gene transcript numbers were
554 standardized and adjusted relative to eukaryotic translation elongation factor 1 alpha 1
555 (*EeF1A1*) transcripts. Gene expression was quantified using the ΔΔCt method. Primers
556 used for RT-PCR were as follows: EeF1A1 Fwd: 5'- TCGGGCAAGTCCACCACTAC -3'
557 and Rev: 5'-CCAAGACCCAGGCATACTTGA-3'; HIF-1α Fwd: 5'-
558 ACTAGCCGAGGAAGAACTATGAA-3' and Rev: 5'-TACCCACACTGAGGTTGGTTA-3';
559 and LDH-A Fwd: 5'-TGGGAGTTCACCCATTAAGC-3' and Rev: 5'-
560 AGCACTCTCAACCACCTGCT-3'.

561

562 **Immunofluorescence analysis**

563 FITC-, PE- or PerCP.Cy5.5-labelled mAbs were used for phenotypic analysis of the
564 following cell-surface receptor repertoires: FITC-anti-CD1a (clone HI149, eBioscience),
565 PE-anti-DC-SIGN (clone 120507, RD System), PerCP.Cy5.5-anti-CD86 (clone 374216,
566 Biolegend), FITC-anti-CD83 (clone HB15e, eBioscience), PE-anti-PD-L1 (clone MIH1,
567 BD Pharmingen) and in parallel, with the corresponding isotype control antibody.
568 Approximately $5x10^5$ cells were seeded into tubes and washed once with PBS. Cells
569 were stained for 30 min at 4ºC and washed twice. Additionally, cells were stained for 40

570 min at 4°C with fluorophore-conjugated antibodies PE-anti-Glut1 (clone 202915 R&D
571 Systems, Minnesota, USA) and in parallel, with the corresponding isotype control
572 antibody. For HIF-1α determination, DCs were permeabilized with methanol and
573 incubated with PE-anti-HIF-1α (clone 546-16, Biolegend). Stained populations were
574 gated according to forward scatter (FSC) and side scatter (SSC) analyzed on FACScan
575 (Becton Dickinson). Isotype matched controls were used to determine auto-fluorescence
576 and non-specific staining. Analysis was performed using the FCS Express (De Novo
577 Software) and results were expressed as median fluorescence intensity (MFI) or
578 percentage of positive cells.
579

580 **Soluble cytokines determinations**

581 Supernatants from DC populations or DC-T cell cocultures were harvested and
582 assessment of TNF-α, IL-10, IL-17A or IFN-γ production was measured by ELISA,
583 according to manufacturers' instructions (eBioscience). The detection limit was 3 pg/ml
584 for TNF-α and IL-17A, 6 pg/ml for IFN-γ, and 8 pg/ml for IL-10.
585

586 **$CD4^+$ T cell activation assay**

587 Specific lymphocyte activation (recall) assays were carried out in cells from tuberculin
588 purified protein derivative-positive skin test (PPD^+) healthy donors by culturing DC
589 populations and autologous T cells at a ratio of 10 T cells to 1 DC in round bottom 96-
590 well culture plates for 5 days as detailed previously[9]. The numbers of DCs were adjusted
591 to live cells before the start of the co-cultures. After 5 days, $CD4^+$ T cell subsets were
592 identified by immunolabeling according to the differential expression of CCR4, CXCR3,
593 and CCR6 as previously reported[73]: $CXCR3^+CCR4^-CCR6^-$ (Th1),
594 $CXCR3^-CCR4^+CCR6^-$ (Th2), $CXCR3^-CCR4^+CCR6^+$ (Th17), and $CXCR3^+CCR4^-CCR6^+$
595 (Th1* or Th1/Th17). The fluorochrome-conjugated antibodies used for flow cytometry
596 analysis were CD4-FITC (clone A161A1, Biolegend), CXCR3-PE-Cy7 (clone G025H7,

597 Biolegend), CCR4-PerCPCy5.5 (clone 1G1, BD Bioscience), CCR6-APC (clone 11A9,
598 BD Bioscience), and CD3-APC-Cy7 (clone HIT3a, Biolegend). A viability dye, Zombie
599 Violet (Biolegend), was used to exclude dead cells. Fluorescence Minus One (FMO)
600 control was used to set proper gating for CXCR3-PE-Cy7, CCR4-PerCPCy5.5, and
601 CCR6-APC detection. Cells were analyzed by fluorescence-activated cell sorting
602 (FACS), using the BD FACSCANTO cytometer and FlowJo™ Software (BD Life
603 Sciences).
604
605 **Chemotactic activity of DCs**
606 Each DC population ($4x10^5$ cells in 75 µl) was placed on the upper chamber of a transwell
607 insert (5 µm pore size, 96-well plate; Corning), and 230 µL of media (RPMI with 0.5 %
608 FCS) with human recombinant CCL21 (200 ng/ml) (Peprotech) was placed in the lower
609 chamber. After 3 h, cells that had migrated to the lower chamber were removed and
610 analyzed. The relative number of cells migrating was determined on a flow cytometer
611 using Calibrite beads (BD Biosciences), where a fixed number of beads was included in
612 each sample and the number of cells per 1,000 beads was evaluated. Data were
613 normalized to the number of initial cells.
614
615 ***In vivo* migration assay**
616 DCs were differentiated from bone marrow precursors obtained from naive BALB/c mice
617 in the presence of murine GM-CSF (10 ng/ml) and IL-4 (10 ng/ml) both from Biolegend
618 for 7 days. After differentiation, DCs were treated with oxamate (20 mM) or PX-478 (10
619 uM) and stimulated with iMtb. After 24 h, DCs were stained with CFSE (5 µM) and
620 inoculated intradermally in the inguinal zone of naïve BALB/c mice. 3 h post-injection,
621 inguinal lymph nodes close to the site of inoculation were harvested and cells were
622 stained with fluorophore-conjugated antibody PE-anti-CD11c (clone HL3, BD
623 Pharmingen). Analysis was performed using the FlowJo Software and results were
624 expressed as the percentage of $CFSE^+/CD11c^+$ cells.

625

626 **3D migration assay**

627 $0.5x10^5$ DCs were seeded on top of fibrillar collagen matrices polymerized from Nutragen
628 2 mg/ml, 10 % v/v MEM 10X (MEM invitrogen, Carlsbad, CA), UltraPure distilled water
629 and 4-6 % v/v bicarbonate buffer (pH=9) 7.5 %. After 24 h, cellular migration was
630 quantified by taking images using an inverted microscope (Leica DMIRB, Leica
631 Microsystems, Deerfield, IL) and the software Metamorph, as described previously[74].
632 Alternatively, in a similar manner, matrices were polymerized using Collagen (Sigma-
633 Aldrich, C9791-10MG) in figure 5C and D. After 24 h of cellular migration, matrices were
634 fixed with paraformaldehyde (PFA) 4 % during 30 min at room temperature and stained
635 with DAPI (Cell signaling). Collagen was removed and membranes were mounted with
636 DAKO. Images were taken by confocal microscopy (FluoView FV 1000), and cells were
637 counted per field.

638

639 **Measurement of cell respiration with Seahorse flux analyzer**

640 Bioenergetics were determined using a seahorse XFe24 analyzer. ATP production rates
641 and relative contribution from the glycolysis and the OXPHOS were measured by the
642 Seahorse XF Real-Time ATP Rate Assay kit. DCs ($2x10^5$ cells/well) were cultured in 3
643 wells per condition. The assay was performed in XF Assay Modified DMEM. Three
644 consecutive measurements were performed under basal conditions and after the
645 sequential addition of oligomycin and rotenone/antimycin (Agilent, USA). Extracellular
646 acidification rate (ECAR) and oxygen consumption rate (OCR) were measured.
647 Mitochondrial ATP production rate was determined by the decrease in the OCR after
648 oligomycin addition. On the other hand, the complete inhibition of mitochondrial
649 respiration with rotenone plus antimycin A, allows accounting for mitochondrial-
650 associated acidification, and when combined with proton efflux rate (PER) data, allows
651 calculation of Glycolysis ATP production rate. All OCR and ECAR values were
652 normalized. Briefly, before the assay brightfield imaging was performed. Cellular area

653 per condition was calculated by ImageJ software and imported into Wave (Agilent) using
654 the normalization function.
655
656 **SCENITH™ assay**
657 SCENITH experiments were performed as previously described[32] using the SCENITH kit
658 containing all reagents and anti-puromycin antibodies (www.scenith.com). Briefly, DCs
659 or PBMCs were treated for 40 min at 37°C in the presence of the indicated inhibitors of
660 various metabolic pathways and puromycin. After the incubation, puromycin was stained
661 using a fluorescently-labeled anti-Puromycin monoclonal antibody (clone R4743L-E8)
662 with Alexa Fluor 647 or Alexa Fluor 488, and analyzed by flow cytometry. For metabolic
663 analysis of monocyte subsets, PBMCs were labeled with PE-anti-CD16 (clone 3G8,
664 Biolegend) and PECy7-anti-CD14 (clone HCD14, Biolegend) mAbs. The impact of the
665 various metabolic inhibitors was quantitated as described[32].
666
667 **Transmission electron microscopy**
668 DCs were fixed in 2.5 % glutaraldehyde / 2 % PFA (EMS, Delta-Microscopies) dissolved
669 in 0.1 M Sorensen buffer (pH 7.2) for 1 h at room temperature, and then preserved in 1
670 % PFA dissolved in Sorensen buffer. Adherent cells were treated for 1 h with 1 %
671 aqueous uranyl acetate then dehydrated in a graded ethanol series and embedded in
672 Epon. Sections were cut on a Leica Ultracut microtome and ultrathin sections were
673 mounted on 200 mesh onto Formvar carbon coated copper grids. Finally, thin sections
674 were stained with 1 % uranyl acetate and lead citrate and examined with a transmission
675 electron microscope (Jeol JEM-1400) at 80 kV. Images were acquired using a digital
676 camera (Gatan Orius). For mitochondrial morphometric analysis, TEM images were
677 quantified with the ImageJ “analyze particles” plugin in thresholded images, with size
678 (μm^2) settings from 0.001 to infinite. For quantification, 8–10 cells of random fields (1000x
679 magnification) per condition were analyzed.

680

681 **Changes of mitochondrial mass**

682 Mitochondrial mass was determined in DCs by fixing the cells with PFA 4% and labeling
683 them with the probe MitoSpy Green FM (Biolegend). Green fluorescence was analyzed
684 by flow cytometry (FACScan, BD Biosciences).

685

686 **GeneSet Enrichment Analysis of human monocytes**

687 BubbleMap analysis was performed with 1,000 geneset-based permutations, and with
688 "Signal2Noise" as a metric for ranking the genes. The results are displayed as a
689 BubbleMap, where each bubble is a GeneSet Enrichment Analysis (GSEA) result and
690 summarizes the information from the corresponding enrichment plot. The color of the
691 Bubble corresponds to the population from the pairwise comparison in which the geneset
692 is enriched. The bubble area is proportional to the GSEA normalized enrichment score
693 (NES). The intensity of the color corresponds to the statistical significance of the
694 enrichment, derived by computing the multiple testing-adjusted permutation-based p-
695 value using the Benjamini–Yekutieli correction. Enrichments with a statistical
696 significance above 0.30 are represented by empty circles.

697

698 **Patient blood donors**

699 TB patients were diagnosed at the División Tisioneumonología, Hospital F.J.Muñiz
700 (Buenos Aires, Argentina) by the presence of recent clinical respiratory symptoms,
701 abnormal chest radiography, and positive culture of sputum or positive sputum smear
702 test for acid-fast-bacilli. Written, informed consent was obtained according to the Ethics
703 Committee from the Hospital Institutional Ethics Review Committee. Exclusion criteria
704 included HIV positive patients and the presence of concurrent infectious diseases or
705 comorbidities. Blood samples were collected during the first 15 days after
706 commencement of treatment. All tuberculous patients had pulmonary TB (Table I). The
707 term symptoms evolution refers to the time period during which a patient experiences

708 cough and phlegm for more than 2-3 weeks, with (or without) sputum that may (or not)
709 be bloody, accompanied by symptoms of constitutional illness (*e.g.,* loss of appetite,
710 weight loss, night sweats, and general malaise).
711

712 **Statistics**

713 All values are presented as the median ± SEM of 3-13 independent experiments. Each
714 independent experiment corresponds to 1 donor. For Seahorse assays, OCR and PER
715 values are shown as mean ± SD. Comparisons between unpaired experimental
716 conditions were made using either ANOVA for parametric data or Friedman test for non-
717 parametric data followed by Dunn's Multiple Comparison Test. Comparisons between
718 paired experimental conditions were made using the two-tailed Wilcoxon Signed Rank
719 Test for non-parametric data or T test for parametric data. Correlation analyses were
720 determined using the Spearman's rank test. A p-value of 0.05 was considered significant.
721

722 **Study approval**

723 *Human specimens.* The study design was reviewed and approved by the Ethics
724 Committees of the Academia Nacional de Medicina (49/20/CEIANM) and the Muñiz
725 Hospital, Buenos Aires, Argentina (NI #1346/21). All participants voluntarily enrolled in
726 the study by signing an informed consent form after receiving detailed information about
727 the research study.

728 *Mouse studies.* All experimental protocols were approved by the Institutional Animal
729 Care and Use of the Experimentation Animals Committee (CICUAL number 090/2021)
730 of the Institute of Experimental Medicine (IMEX, Buenos Aires).
731

732 **AUTHOR CONTRIBUTIONS**

733 Conceptualization & methodology: MM, FF, MFQ, MV, TPVM, CV and LB. Investigation:
734 MM, MJ, ZV, JB, JLMF, MG, SM, MBV, FF, VGP, MV, CV and LB. Resources: SI, RM,
735 LC, PGM, DP, RA, ON, CV, GL-V, MdCS and LB. Formal Analysis: MM, TPVM, and LB.
736 Writing: MM, GL-V, RA, MdCS, ON, CV, TPVM and LB. Visualization: MM, FF, CV,
737 TPVM and LB. Funding acquisition: ON, GL-V, RA, CV, and LB. Corresponding author:
738 LB is responsible for ownership and responsibility that are inherent to aspects of this
739 study.

740

741 **ACKNOWLEDGMENTS**

742 We thank the staff of the Regional Center of Hemotherapy of the Garrahan Hospital
743 (Buenos Aires). We greatly thank Claire Lastrucci for designing the graphical abstract.
744 In addition, we are grateful for the editing service provided by Life Science editors.
745 This work was supported by the Argentinean National Agency of Promotion of Science
746 and Technology (PICT-2019-01044 and PICT-2020-00501 to LB); the Argentinean
747 National Council of Scientific and Technical Investigations (CONICET, PIP
748 11220200100299CO to LB); the Centre National de la Recherche Scientifique,
749 *Université Paul Sabatier*, the *Agence Nationale de Recherche sur le Sida et les hépatites*
750 *virales (ANRS)* (ANRS2018-02, ECTZ 118551/118554, ECTZ 205320/305352, ANRS
751 ECTZ103104 and ECTZ101971 to CV, ON and GL-V); and the French ANR JCJC-Epic-
752 SCENITH ANR-20-CE14-0028 and CoPoC Inserm-transfert MAT-PI-17493-A-04 to RA.
753 The funders had no role in study design, data collection, and analysis, decision to
754 publish, or preparation of the manuscript.

References

1. Weiss, G. & Schaible, U. E. Macrophage defense mechanisms against intracellular bacteria. *Immunological Reviews* **264**, 182–203 (2015).

2. Khader, S. A. *et al.* Interleukin 12p40 is required for dendritic cell migration and T cell priming after Mycobacterium tuberculosis infection. *Journal of Experimental Medicine* (2006) doi:10.1084/jem.20052545.

3. Wolf, A. J. *et al.* Mycobacterium tuberculosis infects dendritic cells with high frequency and impairs their function in vivo. *Journal of immunology (Baltimore, Md. : 1950)* (2007) doi:10.4049/jimmunol.179.4.2509.

4. Cooper, A. M. Cell-Mediated Immune Responses in Tuberculosis. *https://doi.org/10.1146/annurev.immunol.021908.132703* **27**, 393–422 (2009).

5. Lai, R. *et al.* CD11b+ Dendritic Cell–Mediated Anti–Mycobacterium tuberculosis Th1 Activation Is Counterregulated by CD103+ Dendritic Cells via IL-10. *The Journal of Immunology* **200**, 1746–1760 (2018).

6. Urdahl, K. B., Shafiani, S. & Ernst, J. D. Initiation and regulation of T-cell responses in tuberculosis. *Mucosal immunology* **4**, 288–293 (2011).

7. Chandra, P., Grigsby, S. J. & Philips, J. A. Immune evasion and provocation by Mycobacterium tuberculosis. *Nature Reviews Microbiology 2022 20:12* **20**, 750–766 (2022).

8. Ernst, J. D. Mechanisms of M. tuberculosis Immune Evasion as Challenges to TB Vaccine Design. **24**, 34–42 (2018).

9. Balboa, L. *et al.* Monocyte-derived dendritic cells early exposed to Mycobacterium tuberculosis induce an enhanced T helper 17 response and transfer mycobacterial antigens. *International Journal of Medical Microbiology* **306**, 541–553 (2016).

10. Wolf, A. J. *et al.* Initiation of the adaptive immune response to Mycobacterium tuberculosis depends on antigen production in the local lymph node, not the lungs . *The Journal of Experimental Medicine* **205**, 105–115 (2008).

11. Balboa, L. *et al.* Mycobacterium tuberculosis impairs dendritic cell response by altering CD1b, DC-SIGN and MR profile. *Immunol Cell Biol* (2010) doi:10.1038/icb.2010.22.

12. Harding, C. V. & Boom, W. H. Regulation of antigen presentation by Mycobacterium tuberculosis: a role for Toll-like receptors. *Nat. Rev. Microbiol.* **8**, 296–307 (2010).

13. Srivastava, S., Grace, P. S. & Ernst, J. D. Antigen export reduces antigen presentation and limits T cell control of M. tuberculosis. *Cell Host Microbe* **19**, 44–54 (2016).

14. Roberts, L. L. & Robinson, C. M. Mycobacterium tuberculosis infection of human dendritic cells decreases integrin expression, adhesion and migration to chemokines. *Immunology* (2014) doi:10.1111/imm.12164.

15. Rajashree, P., Supriya, P. & Das, S. D. Differential migration of human monocyte-derived dendritic cells after infection with prevalent clinical strains of Mycobacterium tuberculosis. *Immunobiology* **213**, 567–575 (2008).

16. Currivan, E., Finlay, D. & Moreira, D. Dendritic cells metabolism: a strategic path to improve antitumoral DC vaccination. *Clinical and experimental immunology* **208**, 193–201 (2022).

17. Basit, F., Mathan, T., Sancho, D. & De Vries, J. M. Human dendritic cell subsets undergo distinct metabolic reprogramming for immune response. *Frontiers in Immunology* **9**, 2489 (2018).

18. Wculek, S. K., Khouili, S. C., Priego, E., Heras-Murillo, I. & Sancho, D. Metabolic Control of Dendritic Cell Functions: Digesting Information. **10**, 775 (2019).

19. Du, X., Chapman, N. M. & Chi, H. *Emerging Roles of Cellular Metabolism in Regulating Dendritic Cell Subsets and Function*. *Frontiers in Cell and Developmental Biology* vol. 6 (Frontiers Media SA, 2018).

20. Møller, S. H., Wang, L. & Ho, P. C. Metabolic programming in dendritic cells tailors immune responses and homeostasis. **19**, 370–383.

21. Everts, B. & Pearce, E. J. Metabolic control of dendritic cell activation and function: Recent advances and clinical implications. *Frontiers in Immunology* Preprint at https://doi.org/10.3389/fimmu.2014.00203 (2014).

22. Guak, H. *et al.* Glycolytic metabolism is essential for CCR7 oligomerization and dendritic cell migration. *Nat Commun* (2018) doi:10.1038/s41467-018-04804-6.

23. Liu, J. *et al.* CCR7 Chemokine Receptor-Inducible lnc-Dpf3 Restrains Dendritic Cell Migration by Inhibiting HIF-1α-Mediated Glycolysis. *Immunity* **50**, 600-615.e15 (2019).

24. Everts, B. *et al.* TLR-driven early glycolytic reprogramming via the kinases TBK1-IKKε supports the anabolic demands of dendritic cell activation. *Nat Immunol* **15**, 323 (2014).

25. Lawless, S. J. *et al.* Glucose represses dendritic cell-induced T cell responses. *Nature Communications* **8**, (2017).

26. Adamik, J. *et al.* Distinct metabolic states guide maturation of inflammatory and tolerogenic dendritic cells. *Nature Communications 2022 13:1* **13**, 1–19 (2022).

27. Kumar, R. *et al.* Immunometabolism of Phagocytes During Mycobacterium tuberculosis Infection. **6**, 105 (2019).

28. Marín Franco, J. L. *et al.* Host-Derived Lipids from Tuberculous Pleurisy Impair Macrophage Microbicidal-Associated Metabolic Activity. *Cell Rep* (2020) doi:10.1016/j.celrep.2020.108547.

29. Baay-Guzman, G. J. *et al.* Dual role of hypoxia-inducible factor 1 α in experimental pulmonary tuberculosis: Its implication as a new therapeutic target. *Future Microbiology* (2018) doi:10.2217/fmb-2017-0168.

30. Liu, J., Zhang, X., Cheng, Y. & Cao, X. Dendritic cell migration in inflammation and immunity. *Cell Mol Immunol* **18**, 2461–2471 (2021).

31. Freemerman, A. J. *et al.* Metabolic reprogramming of macrophages: glucose transporter 1 (GLUT1)-mediated glucose metabolism drives a proinflammatory phenotype. *The Journal of biological chemistry* **289**, 7884–7896 (2014).

32. Argüello, R. J. *et al.* SCENITH: A Flow Cytometry-Based Method to Functionally Profile Energy Metabolism with Single-Cell Resolution. *Cell Metab* (2020) doi:10.1016/j.cmet.2020.11.007.

33. Quesniaux, V. *et al.* Toll-like receptor pathways in the immune responses to mycobacteria. *Microbes and Infection* **6**, 946–959 (2004).

34. Chow, J. C., Young, D. W., Golenbock, D. T., Christ, W. J. & Gusovsky, F. Toll-like receptor-4 mediates lipopolysaccharide-induced signal transduction. *Journal of Biological Chemistry* **274**, 10689–10692 (1999).

35. Underhill, D. M., Ozinsky, A., Smith, K. D. & Aderem, A. Toll-like receptor-2 mediates mycobacteria-induced proinflammatory signaling in macrophages. *Proceedings of the National Academy of Sciences of the United States of America* **96**, 14459–14463 (1999).

36. Schwandner, R., Dziarski, R., Wesche, H., Rothe, M. & Kirschning, C. J. Peptidoglycan- and Lipoteichoic Acid-induced Cell Activation Is Mediated by Toll-like Receptor 2. *Journal of Biological Chemistry* **274**, 17406–17409 (1999).

37. Koh, M. Y. *et al.* Molecular mechanisms for the activity of PX-478, an antitumor inhibitor of the hypoxia-inducible factor-1α. *Molecular Cancer Therapeutics* **7**, 90–100 (2008).

38. Cairns, R. A., Papandreou, I., Sutphin, P. D. & Denko, N. C. Metabolic targeting of hypoxia and HIF1 in solid tumors can enhance cytotoxic chemotherapy. *Proceedings of the National Academy of Sciences of the United States of America* **104**, 9445–9450 (2007).

39. Kong, D. *et al.* Echinomycin, a Small-Molecule Inhibitor of Hypoxia-Inducible Factor-1 DNA-Binding Activity. *Cancer Research* **65**, 9047–9055 (2005).

40. Cougoule, C. *et al.* Podosomes, But Not the Maturation Status, Determine the Protease-Dependent 3D Migration in Human Dendritic Cells. *Frontiers in immunology* **9**, (2018).

41. Balboa, L. *et al.* Impaired dendritic cell differentiation of CD16-positive monocytes in tuberculosis: Role of p38 MAPK. *Eur J Immunol* (2013) doi:10.1002/eji.201242557.

42. Parlato, S. *et al.* Impaired IFN-α-mediated signal in dendritic cells differentiates active from latent tuberculosis. *PLOS ONE* **13**, e0189477 (2018).

43. Sakhno, L. V. *et al.* Impairments of Antigen-Presenting Cells in Pulmonary Tuberculosis. *Journal of immunology research* **2015**, (2015).

44. McGettrick, A. F. & O'Neill, L. A. J. The Role of HIF in Immunity and Inflammation. *Cell metabolism* **32**, 524–536 (2020).

45. Hillman, H. *et al.* Single-cell profiling reveals distinct subsets of CD14+ monocytes drive blood immune signatures of active tuberculosis. *Frontiers in Immunology* **13**, 1087010 (2023).

46. Spinelli, L., Carpentier, S., Montañana Sanchis, F., Dalod, M. & Vu Manh, T. P. BubbleGUM: Automatic extraction of phenotype molecular signatures and comprehensive visualization of multiple Gene Set Enrichment Analyses. *BMC Genomics* **16**, 1–11 (2015).

47. Reiley, W. W. *et al.* ESAT-6-specific CD4 T cell responses to aerosol Mycobacterium tuberculosis infection are initiated in the mediastinal lymph nodes. *Proceedings of the National Academy of Sciences* **105**, 10961–10966 (2008).

48. Griffiths, K. L. *et al.* Targeting dendritic cells to accelerate T-cell activation overcomes a bottleneck in tuberculosis vaccine efficacy. *Nat Commun* **7**, 1–13 (2016).

49. Harding, J. S., Rayasam, A., Schreiber, H. A., Fabry, Z. & Sandor, M. Mycobacterium-Infected Dendritic Cells Disseminate Granulomatous Inflammation. *Scientific Reports* **5**, (2015).

50. Samstein, M. *et al.* Essential yet limited role for CCR2+ inflammatory monocytes during Mycobacterium tuberculosis-specific T cell priming. *Elife* **2013**, (2013).

51. Semba, H. *et al.* HIF-1α-PDK1 axis-induced active glycolysis plays an essential role in macrophage migratory capacity. *Nature Communications* **7**, 1–10 (2016).

52. Kishore, M. *et al.* Regulatory T Cell Migration Is Dependent on Glucokinase-Mediated Glycolysis. *Immunity* **47**, 875-889.e10 (2017).

53. Park, J. S. *et al.* Mechanical regulation of glycolysis via cytoskeleton architecture. *Nature* **578**, 621–626 (2020).

54. Fernie, A. R., Zhang, Y. & Sampathkumar, A. Cytoskeleton Architecture Regulates Glycolysis Coupling Cellular Metabolism to Mechanical Cues. *Trends Biochem Sci* **45**, 637–638 (2020).

55. Ferreira, G. B. *et al.* Differential protein pathways in 1,25-dihydroxyvitamin d(3) and dexamethasone modulated tolerogenic human dendritic cells. *Journal of proteome research* **11**, 941–971 (2012).

56. Ferreira, G. B. *et al.* Proteome analysis demonstrates profound alterations in human dendritic cell nature by TX527, an analogue of vitamin D. *PROTEOMICS* **9**, 3752–3764 (2009).

57. Basit, F. & de Vries, I. J. M. Dendritic Cells Require PINK1-Mediated Phosphorylation of BCKDE1α to Promote Fatty Acid Oxidation for Immune Function. *Frontiers in Immunology* **10**, 2386 (2019).

58. Ohl, L. *et al.* CCR7 governs skin dendritic cell migration under inflammatory and steady-state conditions. *Immunity* **21**, 279–288 (2004).

59. Krawczyk, C. M. *et al.* Toll-like receptor-induced changes in glycolytic metabolism regulate dendritic cell activation. *Blood* **115**, 4742–4749 (2010).

60. Ryan, R. C. M., O'Sullivan, M. P. & Keane, J. Mycobacterium tuberculosis infection induces non-apoptotic cell death of human dendritic cells. *BMC Microbiol* **11**, 1–13 (2011).

61. Hackett, E. E. *et al.* Mycobacterium tuberculosis Limits Host Glycolysis and IL-1β by Restriction of PFK-M via MicroRNA-21. *Cell Reports* **30**, 124-136.e4 (2020).

62. Martín-Fontecha, A. *et al.* Regulation of Dendritic Cell Migration to the Draining Lymph Node Impact on T Lymphocyte Traffic and Priming. *Journal of Experimental Medicine* **198**, 615–621 (2003).

63. Ziegler-Heitbrock, L. *et al.* Nomenclature of monocytes and dendritic cells in blood. *Blood* **116**, e74–e80 (2010).

64. Ginhoux, F. & Jung, S. Monocytes and macrophages: developmental pathways and tissue homeostasis. *Nature Reviews Immunology* **14**, 392–404 (2014).

65. Wong, K. L. *et al.* Gene expression profiling reveals the defining features of the classical, intermediate, and nonclassical human monocyte subsets. *Blood* **118**, e16–e31 (2011).

66. Cros, J. *et al.* Human CD14dim monocytes patrol and sense nucleic acids and viruses via TLR7 and TLR8 receptors. *Immunity* **33**, 375–386 (2010).

67. Balboa, L. *et al.* Paradoxical role of CD16+CCR2+CCR5+ monocytes in tuberculosis: efficient APC in pleural effusion but also mark disease severity in blood. *J Leukoc Biol* (2011) doi:10.1189/jlb.1010577.

68. Manoharan, I., Prasad, P. D., Thangaraju, M. & Manicassamy, S. Lactate-Dependent Regulation of Immune Responses by Dendritic Cells and Macrophages. *Frontiers in Immunology* **12**, 691134–691134 (2021).

69. Kumar, P. IFNγ-producing CD4+ T lymphocytes: the double-edged swords in tuberculosis. *Clin Transl Med* **6**, 21 (2017).

70. Mootoo, A., Stylianou, E., Arias, M. A. & Reljic, R. TNF-α in tuberculosis: A cytokine with a split personality. *Inflamm Allergy Drug Targets* **8**, 53–62 (2009).

71. Genoula, M. *et al.* Formation of foamy macrophages by tuberculous pleural effusions is triggered by the interleukin-10/signal transducer and activator of transcription 3 axis through ACAT upregulation. *Front Immunol* (2018) doi:10.3389/fimmu.2018.00459.

72. Barham, D. & Trinder, P. An improved colour reagent for the determination of blood glucose by the oxidase system. *The Analyst* **97**, 142–5 (1972).

73. Acosta-Rodriguez, E. V. *et al.* Surface phenotype and antigenic specificity of human interleukin 17–producing T helper memory cells. *Nature Immunology 2007 8:6* **8**, 639–646 (2007).

74. Van Goethem, E., Poincloux, R., Gauffre, F., Maridonneau-Parini, I. & Le Cabec, V. Matrix architecture dictates three-dimensional migration modes of human macrophages: differential involvement of proteases and podosome-like structures. *Journal of immunology (Baltimore, Md. : 1950)* **184**, 1049–1061 (2010).

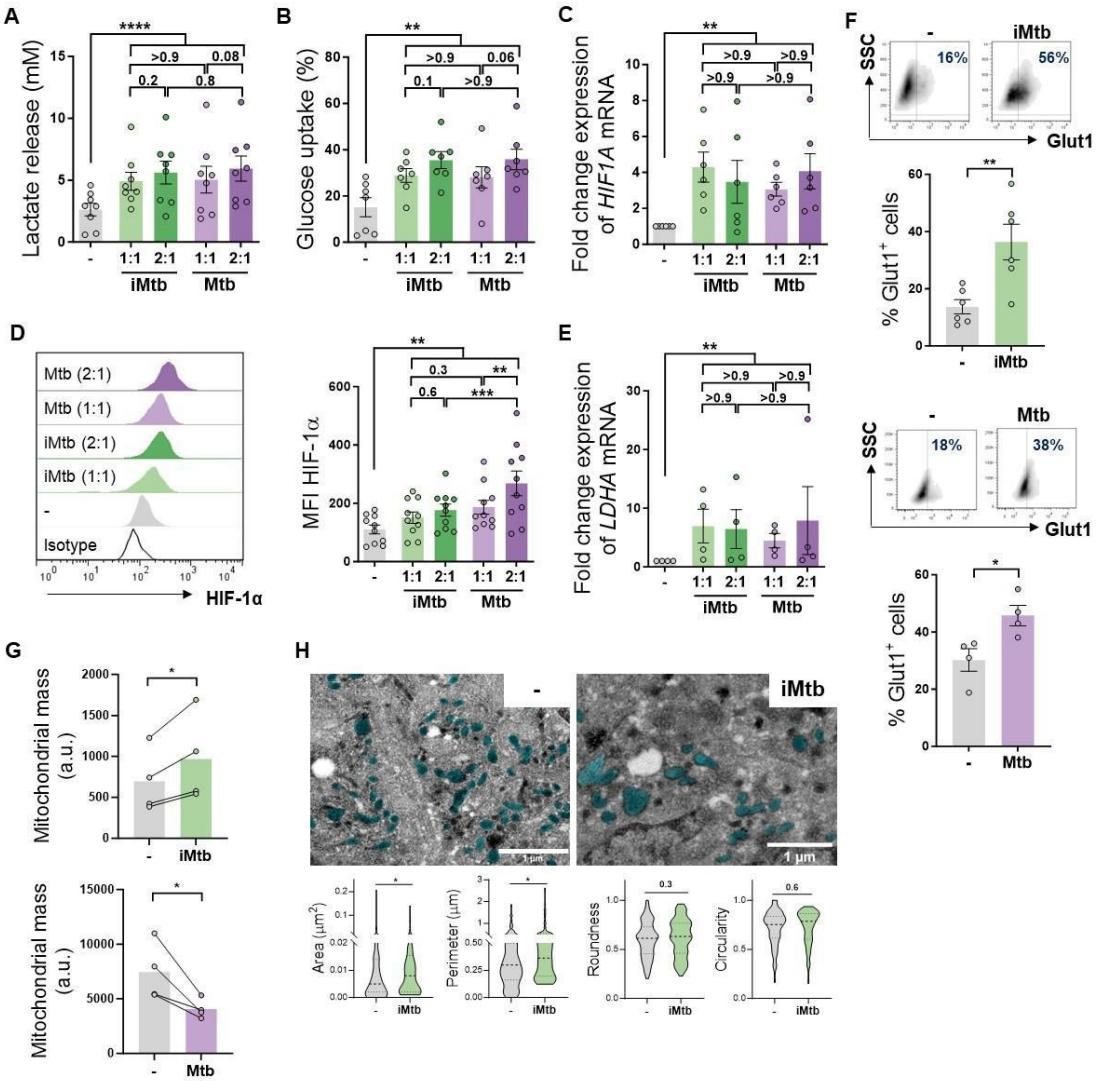

Figure 1. Mtb rewires the metabolic network of monocyte-derived DCs (Mo-DCs). Mo-DCs were stimulated with viable or irradiated Mtb (iMtb) at two MOI (1 or 2 Mtb per DC) for 24 h. Glycolysis was measured as: **(A)** Lactate release in culture supernatants (N=8); **(B)** Glucose uptake measured in culture supernatants (N=7); **(C)** Relative expression of *HIF-1α* mRNA normalized to *EeF1A1* control gene (N=6). **(D)** Representative histograms of the mean fluorescence intensity (MFI) of HIF-1α as measured by flow cytometry. Quantification shown in graph to the right (N=10). **(E)** Relative expression of lactate dehydrogenase A (*LDHA*) mRNA normalized to *EeF1A1* control gene (N=4). **(F)** FACS plots show the percentage of Glut1⁺ cells with and without iMtb stimulation or infected with viable Mtb in a representative experiment. Quantification of Glut1+ cells plotted below (N=4-6). **(G)** MFI of Mitospy probe as a measurement of mitochondrial mass for Mo-DCs treated (or not) with iMtb (upper panel) or infected with viable Mtb (lower panel). The data are represented as scatter plots with each circle representing a single individual, means ± SEM are shown (N=4). **(H)** Representative electron microscopy micrographs of control and iMtb-stimulated DCs showing mitochondria colored in cyan (left panels) and quantified morphometric analysis (right panels) (N=4). Statistical significance was assessed in **(A-E)** using 2-way ANOVA followed by Tukey's multiple comparisons test (∗p < 0.05; ∗∗p < 0.01; ∗∗∗∗p < 0.0001), and in **(F-H)** using paired t test (∗p < 0.05) for iMtb versus controls. All values are expressed as means ± SEM.

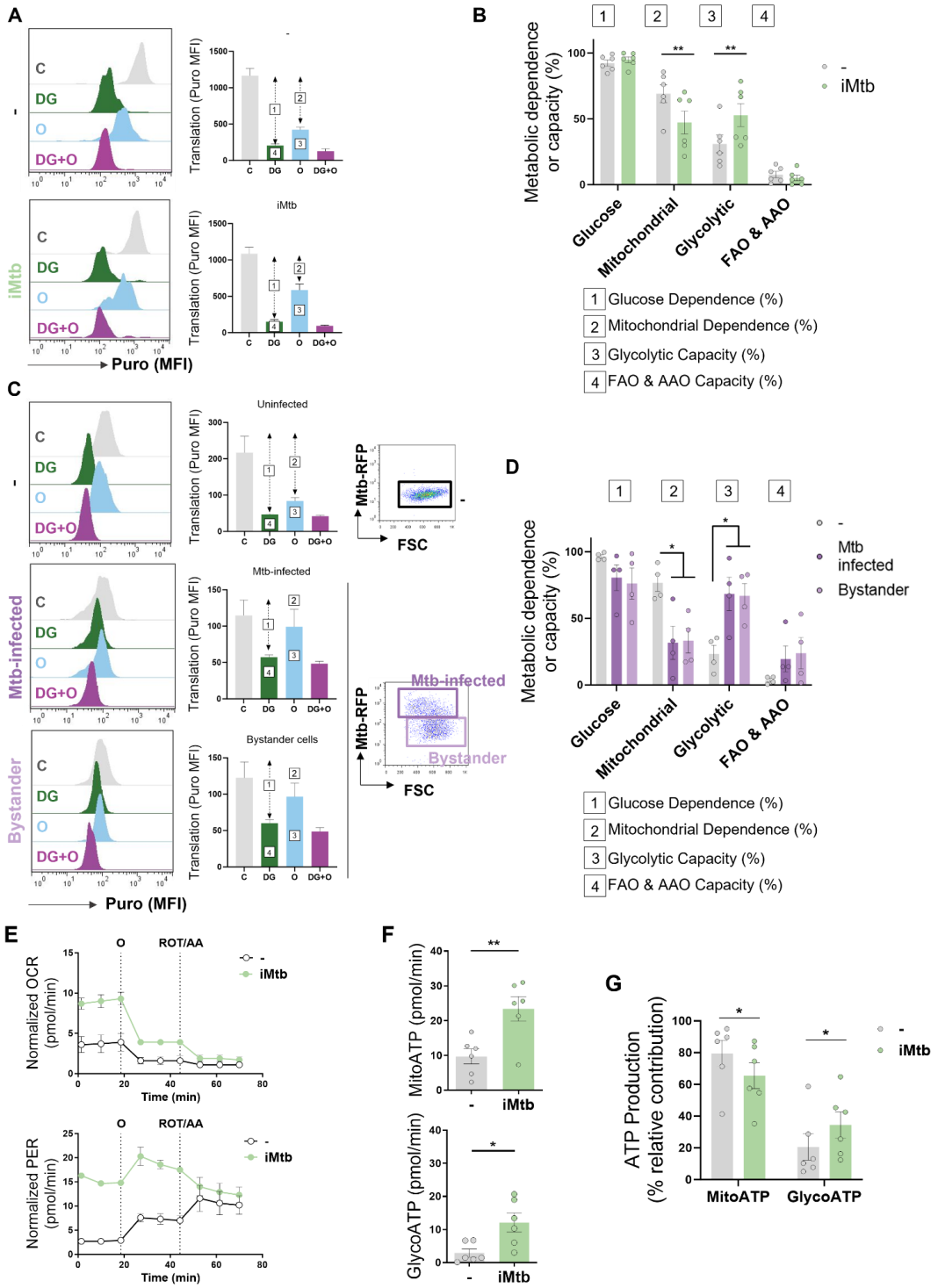

Figure 2. Mtb skews DC metabolism toward glycolysis. Mo-DCs were stimulated with irradiated Mtb (iMtb) or infected with Mtb expressing Red Fluorescent Protein (Mtb-RFP, panel C). **(A)** Representative histograms showing the translation level after puromycin (Puro) incorporation and staining with a monoclonal anti-Puro (anti-Puro MFI) in response to inhibitor treatment (C, Control; DG, 2-Deoxy-D-Glucose; Oligomycin, O; or combination treatment, DG+O). The bar plots show the values of the anti-Puro MFI from 6 donors. Arrows and numbers inside boxes denote the differences between the MFI of puro in the different treatments that are used to calculate the glucose dependence (1) and fatty acids and amino acids oxidation (FAO & AAO) capacity (4); and the mitochondrial dependency (2) and glycolytic capacity (3). **(B)** Relative contributions of glycolytic and FAO & AAO capacities and glucose and mitochondrial dependences to

overall DC metabolism analyzed with SCENITH (N=6)**. (C-D)** DCs were infected with Mtb-RFP for 24 h, thereafter the metabolic profile was evaluated by SCENITH. **(C)** Representative histograms showing the translation level after Puro incorporation are shown for uninfected, Mtb-infected and bystander DCs (those cells that are not infected directly but rather stand nearby). The bar plots show the values of the anti-Puro MFI from 4 donors. Right panel shows representative plots showing the gating strategy to distinguish the populations within Mtb-infected cultures, which includes RFP^+ (Mtb-infected DCs) and RFP^- (bystander DCs) cells. **(D)** Relative contributions of glycolytic and FAO & AAO capacities and glucose and mitochondrial dependences to DC metabolism (N=4). **(E)** Kinetic profile of proton efflux rate (PER; lower panel) and oxygen consumption rate (OCR; upper panel) measurements in control and iMtb-stimulated DCs in response to inhibitor treatments (Oligomycin, O; ROT/AA, Rotenone/Antimycin A), obtained using an Agilent Seahorse XFe24 Analyzer. PER and OCR measurements were normalized to the area covered by cells. **(F)** ATP production rate from mitochondrial oxidative phosphorylation (MitoATP) and glycolysis (glycoATP). MitoATP production rate and glycoATP production rate were calculated from OCR and ECAR measurements in control and iMtb-stimulated DCs (N=6). **(G)** Percentages of MitoATP and GlycoATP relative to overall ATP production (N=6). Statistics in **(B, F-G)** are from paired t test ($*p < 0.05$; $**p < 0.01$) for iMtb versus controls. Statistics in **(D)** are 2-way ANOVA followed by Tukey's multiple comparisons test ($*p < 0.05$) as depicted by lines. The data are represented as scatter plots with each circle representing a single individual, means ± SEM are shown.

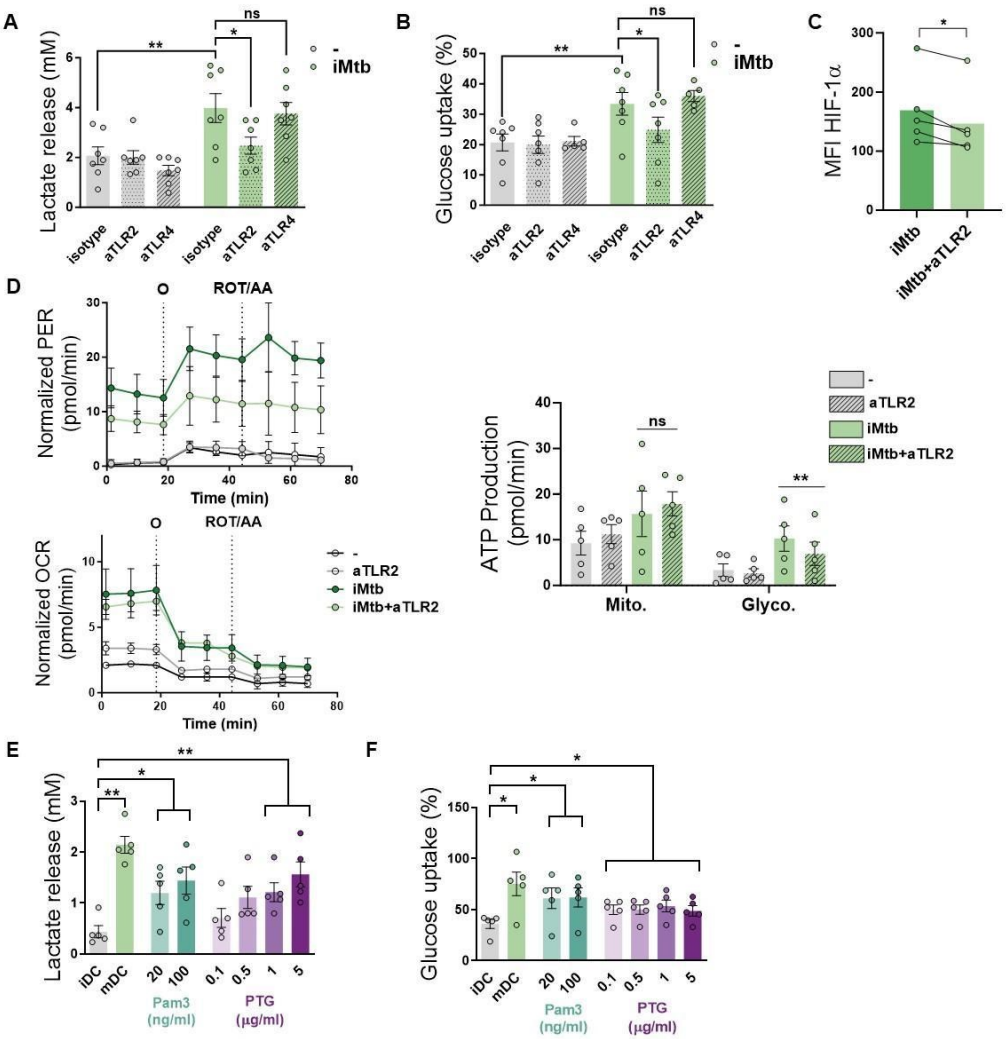

Figure 3. Mtb triggers glycolysis through TLR2 ligation in Mo- DCs. Mo-DCs were stimulated with irradiated Mtb (iMtb) in the presence of neutralizing antibodies against either TLR2 (aTLR2), TLR4 (aTLR4), or their respective isotype controls. **(A)** Lactate release as measured in supernatant (N=7). **(B)** Glucose uptake as measured in supernatant (N=7). **(C)** Mean fluorescence intensity (MFI) of HIF-1α as measured by flow cytometry (N=4). **(D)** Kinetic profile of proton efflux rate (PER) and oxygen consumption rate (OCR) measurements (left panels). Metabolic flux analysis showing quantification of mitochondrial ATP production and glycolytic ATP production (right panel) (N=5). **(E-F)** Mo-DCs were stimulated with Pam3Cys or Mtb peptidoglycan (PTG) at the indicated concentrations. **(E)** Lactate release as measured in supernatant (N=5). **(F)** Glucose uptake as measured in supernatant (N=5). Statistics in **(A-B, E-F)** are 2-way ANOVA followed by Tukey's multiple comparisons test (∗p < 0.05; ∗∗p < 0.01; ∗∗∗∗p < 0.0001). Statistics in **(C-D)** are from paired t test (∗p < 0.05) for iMtb versus controls. The data are represented as scatter plots with each circle representing a single individual, means ± SEM are shown.

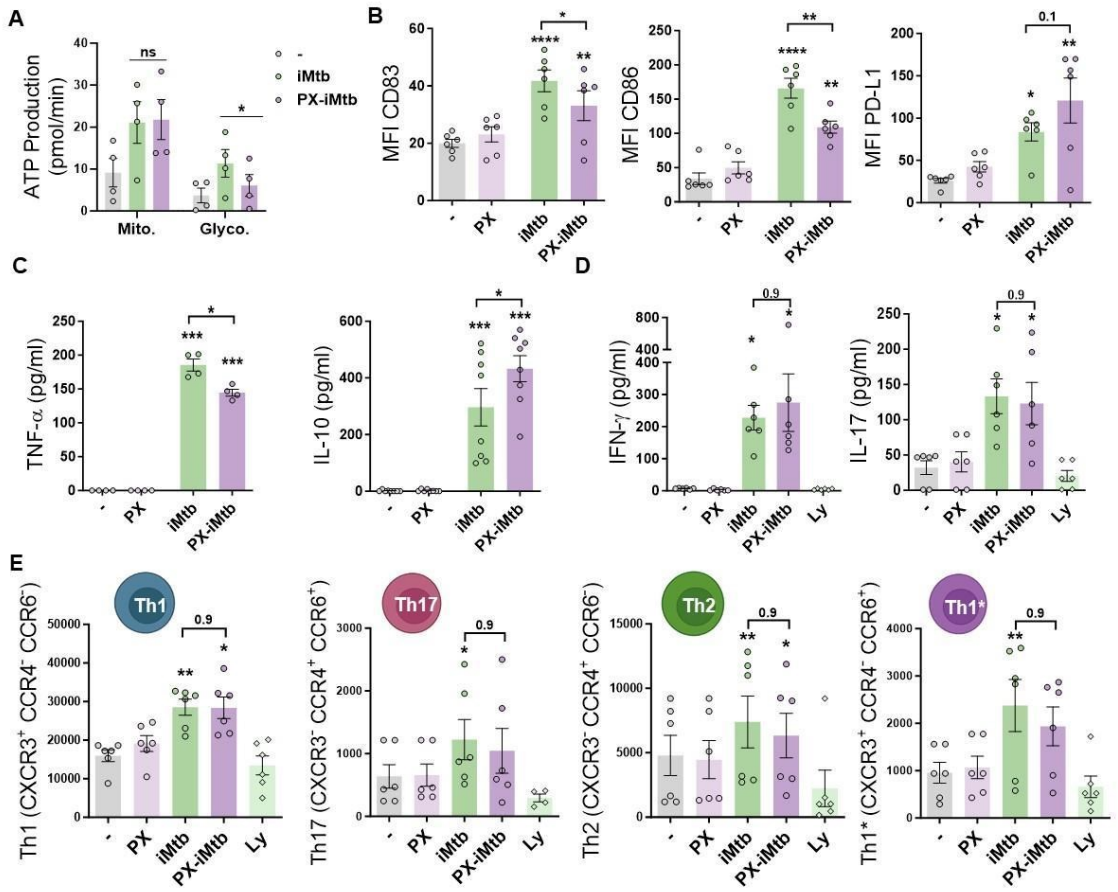

Figure 4. HIF-1α is required for DC maturation upon iMtb stimulation but not for CD4⁺ T lymphocyte polarization. (A-C) Mo-DCs were stimulated with irradiated Mtb (iMtb) in the presence or absence of the HIF-1α inhibitor PX-478 (PX). **(A)** Metabolic flux analysis showing quantification of mitochondrial ATP production and glycolytic ATP production, as in Figure 2C (N=4). **(B)** Mean fluorescence intensity (MFI) of CD83, CD86 and PD-L1 as measured by flow cytometry (N=6). **(C)** TNF-α and IL-10 production by Mo-DCs measured by ELISA (N=4-8). **(D-E)** Monocytes from PPD⁺ healthy donors were differentiated towards DCs, challenged or not with iMtb in the presence or absence of PX for 24 h, washed, and co-cultured with autologous CD4⁺ T cells for 5 days. **(D)** Extracellular secretion of IFN-γ and IL-17 as measured by ELISA (N=6). **(E)** Absolute abundance of Th1, Th17, Th2 and Th1/Th17 CD4⁺ T cells after coculture with DCs (N=6). When indicated lymphocytes without DCs were cultured (Ly). Statistical significance based on 2-way ANOVA followed by Tukey's multiple comparison test (∗p < 0.05; ∗∗p < 0.01). The data are represented as scatter plots with each circle representing a single individual, means ± SEM are shown.

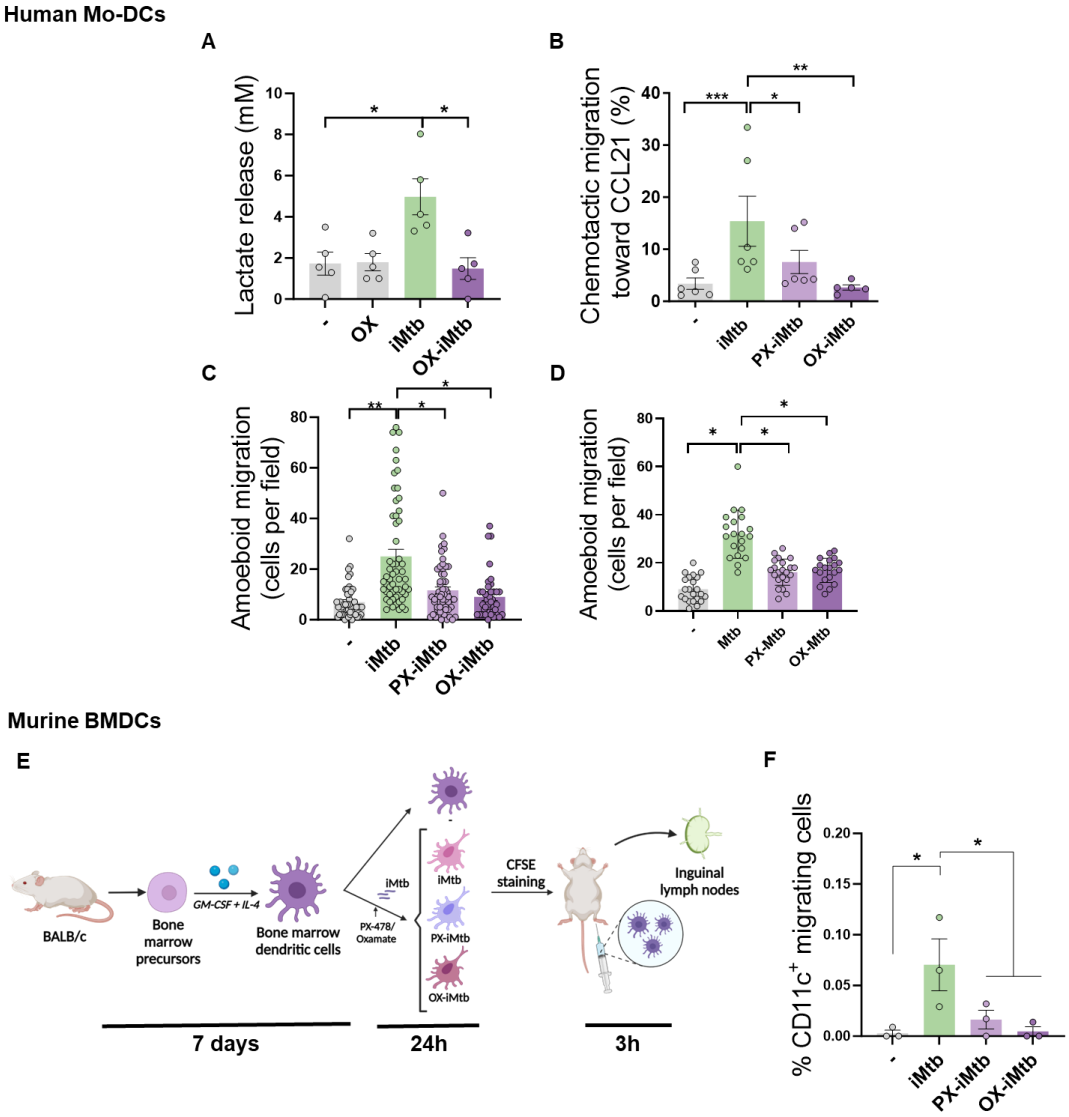

Figure 5. HIF1α-mediated-glycolysis is required to trigger migratory activity in iMtb-stimulated DCs. Mo-DCs were treated (or not) with HIF-1a inhibitor PX-478 (PX) or LDH inhibitor oxamate (OX) and stimulated with iMtb for 24 h. **(A)** Lactate release as measured in supernatants in DCs stimulated or not with iMtb in the presence of OX (N=5). **(B)** Percentage of migrated cells towards CCL21 relative to the number of initial cells per condition (N=6). **(C-D)** Three-dimensional amoeboid migration of DCs through a collagen matrix after 24 h. Cells within the matrix were fixed and stained with DAPI. Images of the membrane of each insert were taken and the percentage of cells per field were counted. **(C)** Mo-DCs stimulated with iMtb for 24 h (N=5). **(D)** Mo-DCs infected with Mtb for 24 h (N=4). The data are represented as scatter plots, where each circle represents a microphotograph sourced from either 5 (C) or 4 (D) independent donors, with each experiment typically including between five to ten microphotographs. **(E)** Representative schematic of the experimental setup for *in vivo* migration assays. **(F)** Percentages of migrating BMDCs (CFSE-labeled among $CD11c^+$) recovered from inguinal lymph nodes (N=3). Statistical significance assessed by **(A-B)** ANOVA followed by Dunnett's multiple comparisons test (∗p < 0.05; ∗∗p < 0.01); **(C-D)** Nested ANOVA followed by Dunnett's multiple comparisons test (∗p < 0.05; ∗∗p < 0.01); **(F)** ANOVA followed by Holm-Sidak's multiple comparisons test (∗p < 0.05).

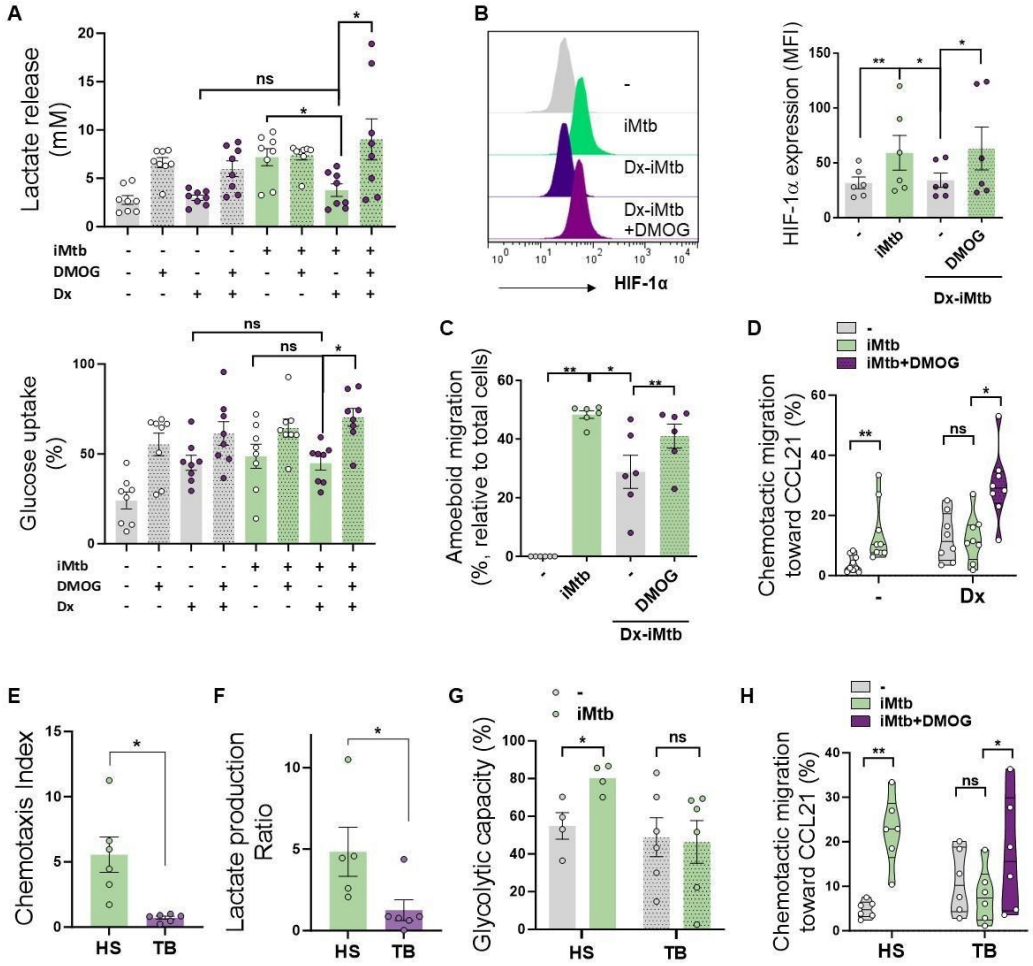

Figure 6. Stabilization of HIF-1α promotes migration of tolerogenic DCs and Mo-DCs from TB patients. Tolerogenic Mo-DCs were generated by dexamethasone (Dx) treatment and were stimulated (or not) with iMtb in the presence or absence of HIF-1α activator DMOG. **(A)** Lactate release and glucose uptake as measured in supernatant (N=8). **(B)** Mean fluorescence intensity (MFI) of HIF-1α. Representative histograms and quantification are shown (N=6). **(C)** Three-dimensional amoeboid migration of DCs through a collagen matrix. After 24 h of migration, images of stacks within the matrix were taken every 30 µm. Percentage of migrating cells were defined as cells in the stacks within the matrix relative to total number of cells (N=6). **(D)** Chemotactic activity towards CCL21 *in vitro* (N=6). **(E-H)** Mo-DCs were generated from healthy subjects (HS) or TB patients, and DCs were stimulated (or not) with iMtb. **(E)** Chemotaxis index towards CCL21 (relative to unstimulated DCs) (N=6). **(F)** Lactate production ratio relative to unstimulated DCs (N=6). **(G)** Glycolytic capacity assessed by SCENITH (N=4). **(H)** Chemotactic activity towards CCL21 of Mo-DCs from TB patients stimulated with iMtb and treated or not with DMOG (N=6). Statistical significance assessed by **(A-D)** 2-way ANOVA followed by Tukey's multiple comparisons test (∗p < 0.05; ∗∗p < 0.01); **(E-G)** Unpaired T test (∗p < 0.05); **(H)** Paired T test (∗p < 0.05). The data are represented as scatter plots with each circle representing a single individual, means ± SEM are shown.

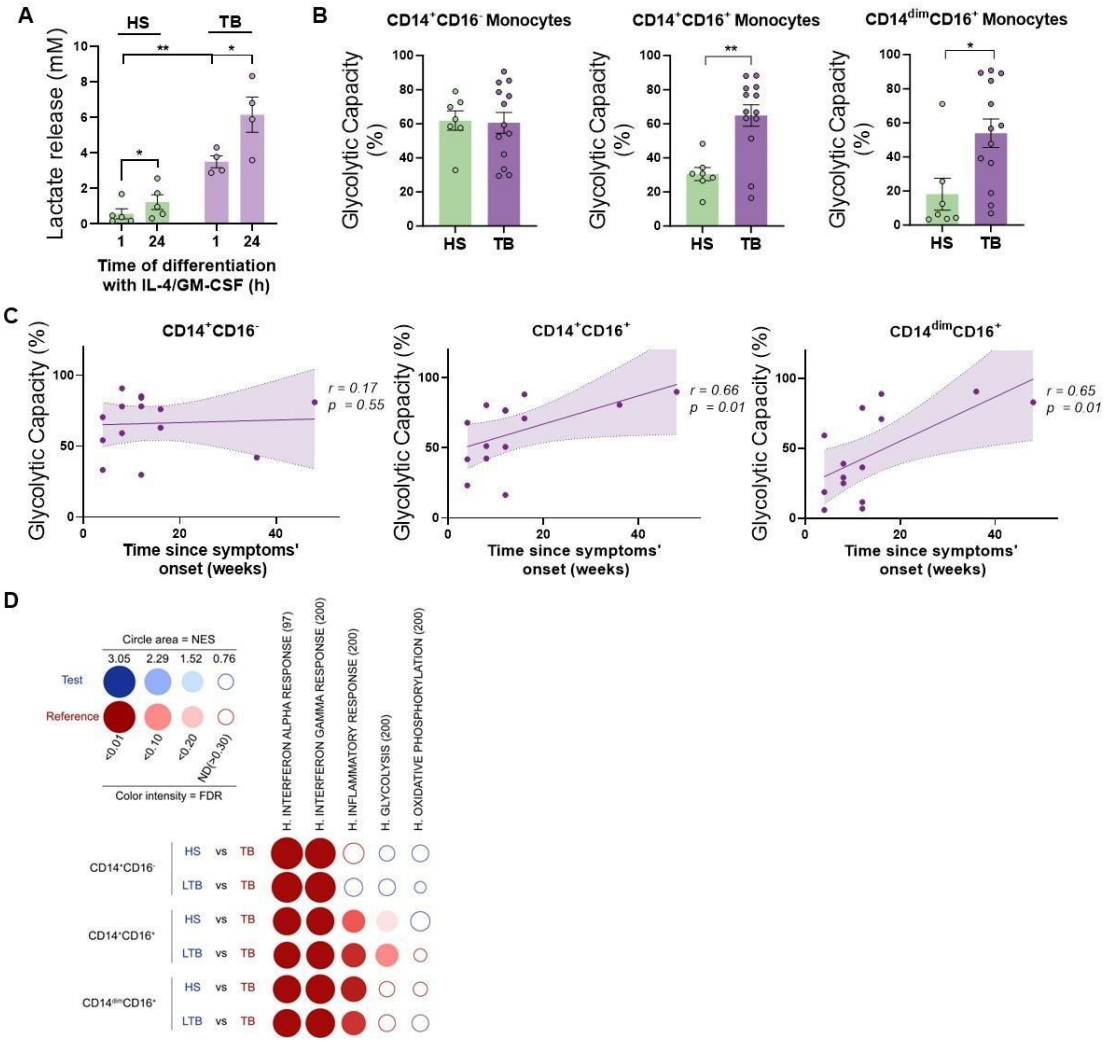

Figure 7. CD16⁺ monocytes from TB patients show increased glycolytic capacity. **(A)** Monocytes from TB patients or healthy subjects (HS) were isolated and cultured with IL-4 and GM-CSF for 24 h. Accumulation of lactate in culture supernatants were measured at 1 and 24 h of differentiation (N=5). (**B**) Glycolytic capacity measured by SCENITH of monocyte subsets as defined by their CD14 and CD16 expression from HS and TB patients (N=7). **(C)** Correlation analysis between the baseline glycolytic capacity and the evolution time of TB symptoms for each monocyte subset ($CD14^{+}CD16^{-}$, $CD14^{+}CD16^{+}$ and $CD14^{dim}CD16^{+}$, N=14). Linear regression lines are shown. Spearman's rank test. The data are represented as scatter plots with each circle representing a single individual, means ± SEM are shown. **(D)** BubbleMap analysis, a high-throughput extension of GSEA, on the pairwise comparisons of monocytes from healthy patients (HS) or donors with latent TB (LTB) vs patients with active TB (TB), for each monocyte subset ($CD14^{+}CD16^{-}$, $CD14^{+}CD16^{+}$ and $CD14^{dim}CD16^{+}$). The gene sets shown come from the Hallmark (H.) collection of the Molecular Signature Database (MSigDB). The colors of the BubbleMap correspond to the population from the pairwise comparison in which the geneset is enriched (red if geneset is enriched in TB). The bubble area is proportional to the GSEA normalized enrichment score (NES). The intensity of the color corresponds to the statistical significance of the enrichment, derived by computing the multiple testing-adjusted permutation-based p-value using the Benjamini–Yekutieli correction. Enrichments with a statistical significance above 0.30 are represented by empty circles. Statistical significance was assessed by **(A)** Paired T test for 0 *vs.* 24h ($*p < 0.05$) and 2-way ANOVA for HS *vs.* TB at each time ($**p < 0.01$); **(B)** unpaired T test ($*p < 0.05$; $**p < 0.01$).

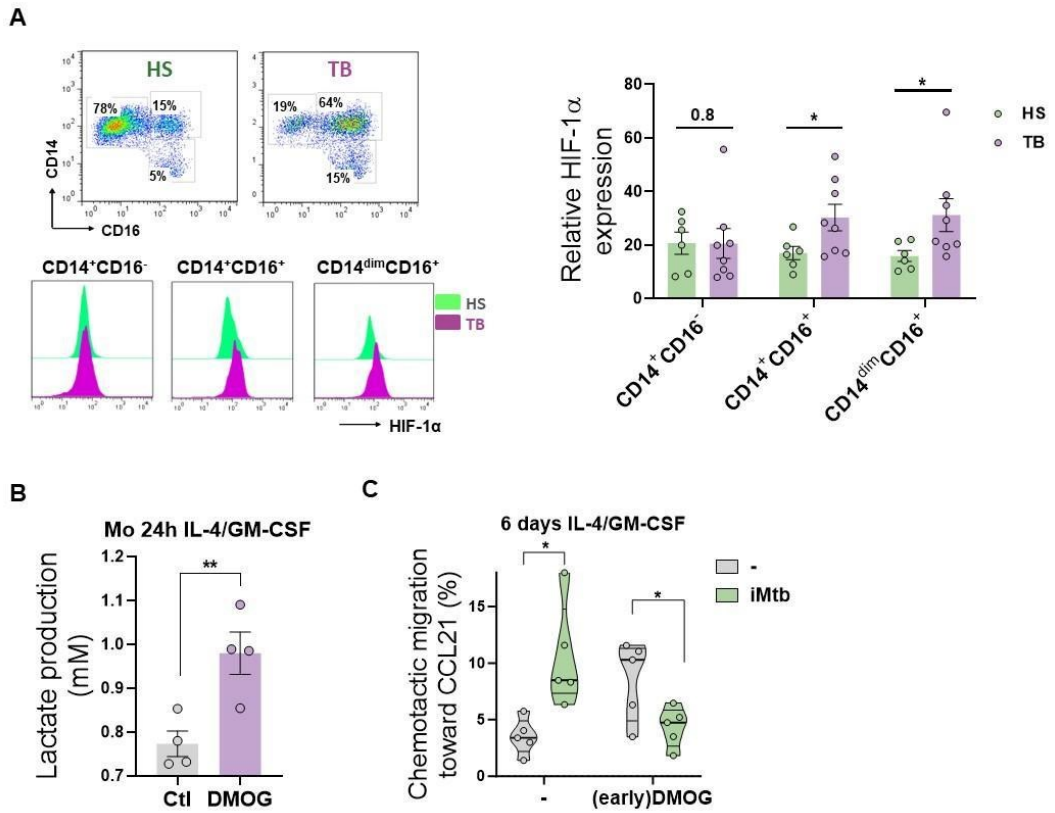

Figure 8. HIF1-α activation in CD16⁺ monocytes from TB patients leads to DCs with poor migration capacity. (A) *Ex-vivo* determination of HIF-1α expression by monocytes from healthy subjects (HS) or TB patients (TB) for each monocyte subset ($CD14^{+}CD16^{-}$, $CD14^{+}CD16^{+}$ and $CD14^{dim}CD16^{+}$) (N=6). **(B-C)** Monocytes from HS were treated with DMOG during the first 24 h of differentiation with IL-4/GM-CSF (earlyDMOG) and removed afterwards. On day 6 of differentiation, cells were stimulated (or not) with iMtb. **(B)** Monocyte lactate release after 24 h of DMOG addition (N=4). **(C)** Chemotactic activity towards CCL21 of DCs (N=5). Statistical significance was assessed by **(B)** paired T test (∗∗$p < 0.01$); **(C)** 2-way ANOVA followed by Tukey's multiple comparisons test (∗$p < 0.05$). The data are represented as scatter plots with each circle representing a single individual, means ± SEM are shown.

Table I. Demographic and clinical characteristics of TB patients

Age, years (range)	36 (19-67)
Gender, % (number/total)	M, 81% (31/38) F, 19% (7/38)
Nationality, % (number/total)	Argentina, 76.31% (29/38) Bolivia, 15.78% (6/38) Paraguay, 2.63% (1/38) Peru, 5.26% (2/38)
TB disease localization, % (number/total)	Pulmonary, 94% (36/38) Pulmonary + Extrapulmonary, 6% (2/38)
AFB* in sputum, % (number/total)	3+, 21% (8/38) 2+, 13% (5/38) 1+, 52% (20/38) -, 13% (5/38)
Leukocyte count, mean ± SEM, cell/µL	8483 ± 509
Lymphocyte mean ± SEM, %	19 ± 2
Monocyte mean ± SEM, %	7 ± 0,5

* Acid-fast-bacilli (AFB) in sputum: -, 1+, 2+, 3+ are defined according to the International Union Against Tuberculosis and Lung Disease (IUATLD)/ World Health Organization (WHO) quantification scale